LONG-TERM STABILITY OF PULTRUDED GLASS FIBER-REINFORCED-POLYMER COLUMNS

by

Qi Guo

Bachelor of Engineering, Tongji University, 2015

Submitted to the Graduate Faculty of

Swanson School of Engineering in partial fulfillment

of the requirements for the degree of

Master of Science

University of Pittsburgh

2017

UNIVERSITY OF PITTSBURGH

SWANSON SCHOOL OF ENGINEERING

This thesis was presented

by

Qi Guo

It was defended on

April 4, 2017

and approved by

Jeen Shang Lin, PhD, Associate Professor

Department of Civil and Environmental Engineering

Qiang Yu, PhD, Assistant Professor

Department of Civil and Environmental Engineering

Kent Harries, PhD, Associate Professor

Department of Civil and Environmental Engineering

Thesis Advisor: Kent Harries, PhD, Associate Professor

Department of Civil and Environmental Engineering

LONG-TERM STABILITY OF PULTRUDED GLASS FIBER-REINFORCED-POLYMER COLUMNS

Qi Guo, M.S.

University of Pittsburgh, 2017

Despite the increasing understanding of long-term behaviors of pGFRP (pultruded Glass Fiber Reinforced Polymer) material, investigation of long-term stability of pGFRP columns is still lacking. In this thesis, the time-dependent axial buckling behavior of pGFRP is investigated – this is termed creep buckling. An equation describing the relationship between mid-height lateral deflection of a section under axial load and time was proposed; this was a modification of traditional viscoelastic models using an empirical model, the Findley power law. Prediction of critical time of creep buckling was determined with the expression and compared to experimental results. For reference, a viscoelastic model utilizing string and dashpot – the Kelvin standard solid model – was also used to obtain theoretical predictions. Model parameters and long-term moduli were determined using flexural creep tests. With comparison between theoretical and experimental results, the equation proposed in this work was observed to offer more conservative and reliable prediction of critical time to creep buckling compared to the analytical equation derived from viscoelastic theory.

TABLE OF CONTENTS

LIST OF TABLES

LIST OF FIGURES

NOMENCLATURE

A_g	gross cross section area
A_i	initial mid-height out-of-straightness of column
a	shear span in flexural tests
b	specimen width
c	constant in Southwell's plot method accounting for imperfections
d	specimen depth (thickness)
E	elastic modulus
$\underline{E}$	viscoelastic differential operator
E_0	initial elastic modulus
E_1	elastic modulus of spring representing creep behavior in Kelvin model
E_t	material parameter in Findley power law
E_{1000}	elastic modulus at 1000 hours of loading
E_∞	long-term (infinite) elastic modulus
e	eccentricity of applied axial load
$f^K(t)$	deflection ratio function based on Kelvin model
$f^F(t)$	deflection ratio function based on Findley model
G_{LT}	in-plane shear modulus

I	moment of inertia
I_{min}	weak axis moment of inertia
K	effective length factor
L	specimen length
M	moment of applied load
M_0	moment of lateral force on columns
m	dimensionless material-specific parameter
m'_F	Findley material parameter
n	dimensionless Findley material parameter
n_s	shape factor of shear
P	applied load
P_{cr}	critical load
P_e	modified critical load
P_E	Euler critical load
P_{E_0}	Euler critical load with initial longitudinal modulus
P_{E_∞}	Euler critical load with infinite longitudinal modulus
P_{E_t}	Euler critical load with creep parameter in Findley model
P_{exp}	experimental critical load
P_f	load of free weight hanger
P_i	load of top roller support
P_{ult}	ultimate failure load in flexural tests
r	radius of gyration

t	time
t_o	time of initial loading
v	lateral deflection of columns
v_0	initial deflection of columns
v_c	creep deflection of columns
w	load of free weight
y	neutral axis position
α	neutral axis position normalized to depth of specimen; i.e.: $y = \alpha d$
β	material parameter
δ	mid-height lateral deflection of columns
ε	strain
ε_0	initial elastic strain
ε'_{o_F}	Findley material parameter
ε_c	creep strain
ε_1	strain of second unit in Kelvin model
η	viscosity of the dashpot in Kelvin model
λ	reciprocal of τ_r in Kelvin model
λ	applied load/buckling load (Bennett's equation)
μ	magnification factor
σ	stress
σ_{m_F}	Findley material parameter
σ_{ε_F}	Findley material parameter

τ_d	Kelvin model parameter
τ_r	retardation time
$\psi(t)$	creep function

All values and equations in thesis are intended to be given in consistent SI units. Where these have been converted from US Standard units, the following factors are used:

1 mm = 0.0394 in

1 N = 0.225 lbf

1 kg = 2.205 lbf

1 MPa = 145 psi

ACKNOWLEDGEMENT

I would like to acknowledge the assistance and support from the following people throughout this research.

Firstly, I would like to thank my advisor, Dr. Kent Harries, for his constant encouragement, patience and guidance. I also appreciate the time devoted by the committee members Dr. Qiang Yu and Dr. Jeen-Shang Lin and their inspiring comments.

Thanks to Charles Hager, the lab technician, who made the experimental work a lot more efficient and pleasant. Thanks to Tianqiao Liu, for his generous help in my tests and thesis review.

I would also like to thank my boyfriend Bing Han, my friends and family, for their endless love and encouragement.

1.0 INTRODUCTION

1.1 RESEARCH BACKGROUND

Over the past few decades, the application of Fiber Reinforced Polymer (FRP) has grown from the aerospace and automotive industries to be widely used in the construction industry. This transformation largely resulted from manufacturing efficiencies realized using pultrusion which reduced the cost and increased the speed of manufacture. Pultrusion is a continuous forming process in which continuous fibers are saturated with a liquid polymer resin and pulled through a heated die to form a desired shape. The shape is rapidly cured at elevated temperature and the resulting rigid section is pulled and cut by a saw to the desired length. With increasing understanding of the material's structural capacity, the role that pultruded glass fiber reinforced polymer (pGFRP) materials play in construction has gone beyond non-structural components to structural elements, particularly when these are located in corrosive environments. With advantages such as light weight and versatility of the shapes that may be formed, pGFRP materials have also been widely used for strengthening existing structures using less labor and time cost. Another competitive property of FRP materials is their resistance to corrosion, which is significant especially for marine structures or other structures exposed to corrosive environments such as cooling towers and agricultural facilities. Benefits of FRP materials also include their anisotropic behaviors which allow specific requirements of high strength or stiffness to be designed into the

product. However, the anisotropic nature of pGFRP is generally seen as a disadvantage in structural applications which would otherwise use isotropic materials such as steel. The anisotropy adversely affects connection design (e.g., Cunningham et al. 2015) and buckling behavior (e.g., Vieira et al. 2017). Additionally, FRP materials are considered brittle, behaving in an essentially linear elastic manner until catastrophic failure. As a result, material utilization (efficiency) is often lower than with isotropic materials, Nonetheless, FRP materials are considered as being competitive in civil engineering industries particularly in applications where corrosion resistance is critical.

Nonetheless, popularization of pGFRP materials is impeded by the lack of complete understanding of their structural behaviors, which leads to restricted specification for design and construction. One of the most significant aspects for which there is little data is the long term performance of pGFRP materials. Understanding mechanical degradation such as fatigue and creep are critical for designers to decide the lifetime of structures, which influences the cost for structural maintenance. Due to limited knowledge about long-term pGFRP material behavior, many applications in civil engineering are limited due to the conservative consideration of creep. More precise predictions of creep behavior are needed to improve the economy of pGFRP structural design in the future.

Creep and buckling have been investigated by researchers since the 1950s. On one hand, different descriptive models were proposed such as the Schapery single integral procedure (R. A. Schapery, 1969) and the Findley power law (Findley,1956). Most of the models were based on viscoelastic theory since creep of pGFRP composites was considered to result from creep of the viscoelastic resin material. On the other hand, experimental studies have been conducted for pGFRP composites in various forms such as full-scale beams, columns and coupons from those

structural members. Both flexural and compressive creep tests were conducted and the latter included both short-term and long-term tests on slender columns and short stubs. Nonetheless, there was little work about prediction of critical buckling time of pGFRP slender columns.

1.2 RESEARCH SCOPE AND OBJECTIVE

This study will focus on the creep behaviors of pGFRP (pultruded Glass Fiber Reinforced Polymer), especially the global buckling of slender pGFRP columns caused by creep. The goal is to verify a theoretical prediction of critical time for creep buckling of pultruded GFRP columns. The prediction is based on the Findley power law, an empirical model describing FRP creep behaviors (Findley 1956). Besides the Findley power law, the Kelvin standard solid model (Bazant, 2010) is applied and compared with experimental results.

Experimental work including flexural creep tests and creep buckling tests is presented. For the flexural creep tests, six pultruded GFRP prismatic beams were loaded at three stress levels for 1,000 hours. From the flexural test results, long-term moduli required for the predictive creep equations based on the Kelvin model and Findley power law can be obtained. The long-term modulus is used in turn predict the critical buckling time for slender specimens subject to concentric compressive loads at 92% of the static (or short term) buckling load. Evaluation of the predictive capacity of the proposed equations through comparison with experimentally-determined critical buckling time is made.

2.0 LITERATURE REVIEW

In this chapter, the two descriptive models, the Findley power law and Kelvin standard solid model are reviewed. Then, previous research about creep behavior of pGFRP composites including experimental and analytical work is discussed. Finally the relationship between stability of pGFRP columns and their susceptibility to material creep is described. Since creep of pGFRP composites results from their viscoelastic properties, it is normally influenced by several environmental factors such as temperature. This thesis focuses only on the creep process in an ambient laboratory environment.

2.1 FUNDAMENTALS OF CREEP BEHAVIOR

Creep is time-dependent deformation under constant applied stress. The mechanism for creep is different for different materials such as metals, polymers or concrete. But generally, the creep process is considered to include three stages: primary creep, secondary creep and tertiary creep (Figure 2.1). ε_0 is the elastic (initial) strain associated with a constant applied stress. The primary stage begins immediately after loading, during which deformation increases initially rapidly and slows down with time. In the secondary creep phase, deformation is almost uniform. In the tertiary stage, deformation will increase quickly again till the material fails. The length of each stage

depends on the level of applied load. At lower applied loads (relative to the long-term buckling capacity), the tertiary stage will not develop.

For pGFRP materials, the physical mechanisms of creep at relatively low loads depends primarily on the polymer matrix, which is usually viscoelastic material. Physical models describing such materials include linear viscoelastic models such as the Kelvin standard solid model and other rheological models such as Kelvin chains (Bazant, 2010) as well as non-linear viscoelastic models such as the Schapery single integral process (Schapery, 1969). The glass reinforcement of a pGFRP is also a viscoelastic material and affects creep behavior, typically at greater loads. Since both primary components of a pGFRP material are viscoelastic, a measure of their relative proportion, typically the fiber volume ratio, will also be required to fully describe creep behavior. In practice, creep behavior of pGFRP is most often considered empirically, with the composite material being treated a single viscoelastic bulk material.

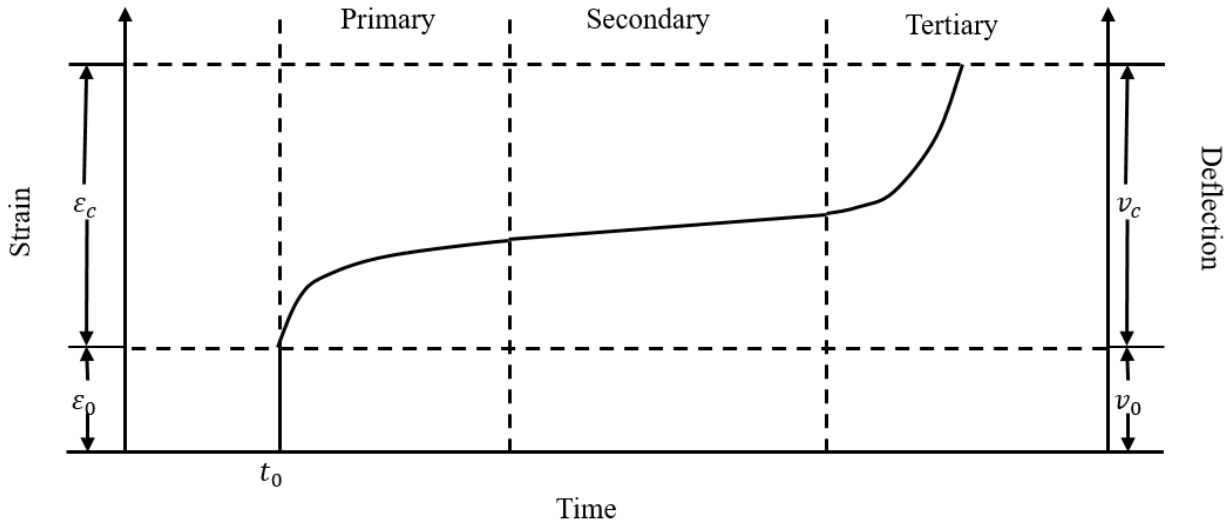

Figure 2.1 The three stages in creep process

2.2 GFRP CREEP CHARACTERIZATION

There are generally three types of models for the characterization of pGFRP creep behaviors. Empirical models such as the Findley power law (Findley 1956) have no physical or mechanical significance but fit well with test results. The second type, of which the Kelvin standard model Bazant, 2010) is an example, is usually composed of mechanical elements which have physical significance but are not specific to a certain material. The springs and dashpots in such models represent elasticity and viscosity respectively, and multiple elements are combined to describe the viscoelasticity exhibited by pGFRP composites or any other viscoelastic material. The third model type is normally more detailed in terms of representing modulus and will typically be limited in application range (Horvath 1998). The constitutive equations of creep in all models take the basic form:

$$\varepsilon = \varepsilon_0 + \varepsilon_c \tag{2.1}$$

where ε_0 is the instantaneous time-independent strain, ε_c is the time-dependent (creep) strain and ε is the total strain as shown schematically in Figure 2.1.

2.2.1 Findley power law

Before the Findley power law, there had been several mathematical expressions proposed to describe creep behavior; each adopted a different non-linear relationship between strain and time (Table 2.1).

Table 2.1 Early mathematical expressions for creep behavior

Reference	Expression
Leaderman (1939)	$\varepsilon = \varepsilon_0 + \mathrm{A}\log t + Bt + \mathrm{C}$
Cottrel and Aytekin (1947)	$\varepsilon = \varepsilon_0 + At^{1/3} + Bt$
Pao and Marin (1952)	$\varepsilon = \varepsilon_0 + A(1 - e^{-Ct}) + Bt + D$

In 1956, Findley put forward a power law expression and proved its ability to characterize creep in unfilled thermoplastic materials by testing three types of plastics for 500 hours (Findley, 1956). The model was widely adopted and considered to be a reliable empirical expression. It is recommended by the *ASCE Structural Plastic Design Manual* (ASCE 1984). Based on the basic creep constitutive form shown as Equation 2.1, the assumption was made by Findley and Khosla (1956) that

$$\varepsilon_c = m\left(\frac{t}{t_o}\right)^n \tag{2.2}$$

In Equation 2.2, which is a power law function, t_o is a time unit that has usually been omitted in subsequent research; m is a dimensionless material-specific parameter; and n is a dimensionless Findley material parameter. Equation 2.1, therefore becomes:

$$\varepsilon = \varepsilon_0 + mt^n \tag{2.3}$$

In most of the previous work utilizing the Findley power law for creep prediction, Equation 2.3 was usually written in the form of a logarithm:

$$\log(\varepsilon - \varepsilon_0) = n\log t + \log m \tag{2.4}$$

Equation 2.4 is a linear function of $\log(\varepsilon - \varepsilon_0)$ and $\log t$ in which constants n and m become the slope and intersection of the function, respectively, which makes it easier to estimate model parameters. Equation 2.3 is not the complete expression of the Findley power law but only a

general power law model. The complete Findley equation consists of the assumption for ε_0 and m that

$$\varepsilon_0 = \varepsilon'_{o_F} \sinh\left(\frac{\sigma}{\sigma_{\varepsilon_F}}\right) \tag{2.5}$$

$$m = m'_F \sinh\left(\frac{\sigma}{\sigma_{m_F}}\right) \tag{2.6}$$

which has five model parameters: ε'_{o_F}, m'_F, σ_{ε_F}, σ_{m_F} and σ. The first four are Findley material parameters and σ is the applied stress. The resulting hyperbolic relationship is based on activation energy theory, which is in the realm of micromechanics. It also represents the assumption about the rheological behavior of polymeric material under tensile stress (Findley et al. 1956). Substituting Equations 2.5 and 2.6 into 2.4 yields:

$$\varepsilon = \varepsilon'_{o_F} \sinh\left(\frac{\sigma}{\sigma_{\varepsilon_F}}\right) + m'_F \sinh\left(\frac{\sigma}{\sigma_{m_F}}\right) t^n \tag{2.7}$$

Following the introduction of the original Findley model, modifications were proposed. Chambers (1984) proposed simplification of Equation 2.6. According to Equation 2.4, it is necessary that initial strain be proportional to applied stress. However the relationship should be close to linear when $\sigma/\sigma_{\varepsilon_F}$ is sufficiently small, indicating that the applied load is small compared to failure load of the material. Chambers utilized this concept, omitted the hyperbolic function, and proposed the following simplified Findley equation.

$$\varepsilon = \varepsilon'_{o_F} \left(\frac{\sigma}{\sigma_{\varepsilon_F}}\right) + m'_F \left(\frac{\sigma}{\sigma_{m_F}}\right) t^n \tag{2.8}$$

On the basis of Equation 2.7, Chambers made further modifications noting that:

$$E_0 = \frac{\sigma_{\varepsilon_F}}{\varepsilon'_{o_F}} \tag{2.9}$$

$$E_t = \frac{\sigma_{m_F}}{m'_F} \tag{2.10}$$

Chamber defined E_{o_F} as a constant linear-elastic modulus or Young's modulus for initial loading and E_t as a constant modulus for creep behaviors. Thus Equation 2.7 became:

$$\varepsilon = \frac{\sigma}{E_0} + \frac{\sigma}{E_t} t^n = \sigma \left(\frac{1}{E_0} + \frac{t^n}{E_t} \right) = \frac{\sigma}{E(t)} \tag{2.11}$$

In which $E(t)$ is a time-dependent Young's modulus.

2.2.2 Kelvin standard solid model

Before discussion of the Kelvin standard solid model, it is necessary to introduce two basic viscoelastic models, the Kelvin-Voigt and Maxwell models shown in Figure 2.2 (Bazant, 2010).

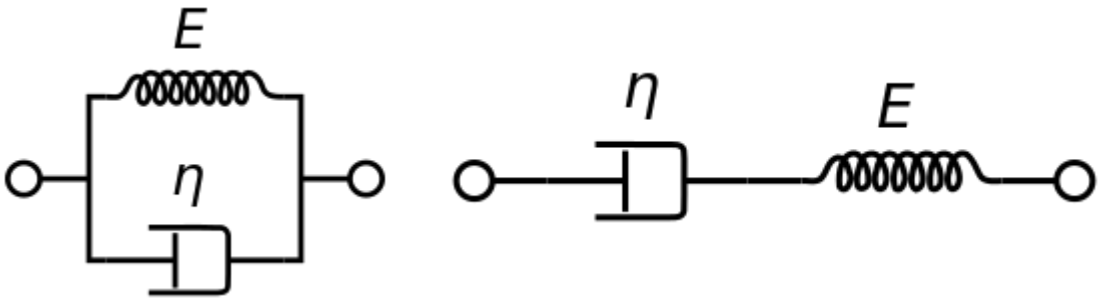

Figure 2.2 Schematic representations of the Kelvin-Voigt (left) and Maxwell models (right)

Both models contain a spring and a dashpot as a unit. The spring represents elastic stress which depends on strain, and the dashpot represents viscous stress which depends on strain rate. The connection between mechanical elements is similar to the concept of an electric circuit. Stress is analogous to electric current and strain to voltage. That is to say, all of the stress is the same for

elements in series and strain is the same for elements in parallel. In the Kelvin-Voigt model, the spring and dashpot are parallel, which resembles the mechanism of creep. And in the Maxwell model, the spring and dashpot are in series, which represent the mechanism of stress relaxation. Although the Kelvin-Voigt model is able to describe creep, it cannot define the behavior of pGFRP composites since there is an elastic period during the loading. Thus more elements are needed for a better prediction of creep in pGFRP composites.

The Kelvin standard solid model is a three-parameter rheological model based on linear viscoelasticity theory. It is composed of one spring in series with a Kelvin unit. (Figure 2.3) The spring E_0 captures the instantaneous behavior of pGFRP composites during loading and the subsequent creep depends on the Kelvin unit.

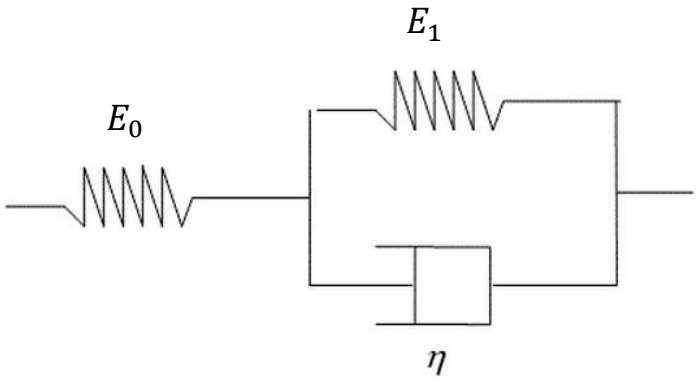

Figure 2.3 Schematic representations of the Kelvin standard solid model.

According to Figure 2.3, the relationship of stress, stain and strain rates can be expressed as Equations 2.12-2.14.

$$\sigma = E_0\varepsilon_0 = E_1\varepsilon_1 + \eta\dot{\varepsilon}_1 \tag{2.12}$$

$$\varepsilon = \varepsilon_0 + \varepsilon_1 \tag{2.13}$$

$$\dot{\varepsilon} = \dot{\varepsilon_0} + \dot{\varepsilon_1} \tag{2.14}$$

After rearranging, the differential equation for strain is obtained:

$$(E_0 + E_1)\sigma + \eta\dot{\sigma} = E_0 E_1 \varepsilon + E_0 \eta \dot{\varepsilon} \tag{2.15}$$

Solving Equation 2.15 yields the time-dependent constitutive equation:

$$\varepsilon(\mathrm{t}) = \frac{\sigma}{E_0}\left(\frac{E_0 + E_1}{\eta}\frac{\left(1 - e^{-\lambda t}\right)}{\lambda} + e^{-\lambda t}\right) \tag{2.16}$$

In Equation 2.17, $\lambda = \frac{E_1}{\eta} = \frac{1}{\tau_r}$. τ_r is the retardation time, which measures the time for creep strain to accumulate. The shorter the retardation time, the more rapid the creep strain development. There are two parameters E_1 and η in the expression which can be determined through curve fitting of experimental strain data. E_0 is the initial elastic modulus. When time approaches infinity, the strain at infinity becomes:

$$\varepsilon_\infty = \sigma\frac{E_0 + E_1}{E_0 E_1} = \frac{\sigma}{E_\infty} \tag{2.17}$$

in which E_∞ is the infinite longitudinal modulus. Substituting λ into Equation 2.16 could modify the expression of time-dependent strain into a function with two unknown parameters, τ_r and E_∞.

$$\frac{\varepsilon(\mathrm{t})}{\sigma} = \frac{1}{\mathrm{E(t)}} = [\frac{1}{E_\infty} - \left(\frac{1}{E_\infty} - \frac{1}{E_0}\right) * e^{-\frac{t}{\tau_r}}] \tag{2.18}$$

2.3 GFRP CREEP BEHAVIORS

Holmes and Rahman (1980) presented 15,000-hour flexural creep tests on three pGFRP box beams. The size of the beams was 150 x 300 x 6000 mm and diaphragms with a spacing of 500 mm were included to increase stiffness. Four-point loading was applied. Two beams were loaded

with 500 kg at each loading point which was approximately 1/3 the ultimate failure load; the third beam only supported its own weight as a reference specimen. For the two beams under the same load, beam 1 bore constant load while beam 2 experienced alternating loads (cyclic loading and unloading in the first 2000 hours then permanent loads in the remainder of the test. Tensile, compressive and shear strains were tracked with time and mid-span deflection was measured constantly. Through the curve of creep deflection, 74.2% of the total 15,000 hour creep was observed to occur in the first 1,000 hours. When tests were done, the authors utilized several mathematical equations including the Findley power law and verified the agreement between prediction and experimental results of beam 1. Good correlation was observed between tensile strain and Findley power law predictions although none of the equations fitted the compressive strain data. It was hypothesized that the inconsistent compression data might result from the occurrence of local buckling and creep recovery during tests.

Daniali (1991) explored flexural creep of pGFRP T-shape beams experimentally based only on deflection change. Several factors affecting pGFRP creep were taken into account in the tests including web shape (solid web and cavity web), binder type (polyester and vinylester) and temperature (ambient condition and elevated temperature at 54^{o}C). Through multiple creep tests up to 10,000 hours, Daniali reports better resistance to strength reduction for vinylester resin during creep. At elevated temperature, beams made from both resin materials exhibited greater creep rates, Polyester beams exhibited greater creep rates at higher temperature. All types of beams failed due to buckling: lateral torsional buckling in solid-web beams and web buckling in cavity-web beams. Solid-web beams showed lower critical load than cavity-web beams in destructive tests.

Bank and Mosallam (1993) investigated creep and failure of a full-size pGFRP frame experimentally and made comparison between test results and theoretical predictions using the Findley power law. One-quarter of the frame failure load was applied. Readings of both flange and web strain allowed consideration of shear deformations and Timoshenko beam theory to be included in the long-term behavior analysis of frame. 10,000-hour strain and deflection data was recorded (Mosallam, 1990; Mosallam and Bank, 1991) and significant creep occurred in approximately the first 2000 hours. A conclusion was made that viscoelastic axial modulus decreased by 35% and shear modulus by 45% in ten years, which suggested the great influence of creep to pGFRP properties as well as the significance of the shear contribution to pGFRP frame behavior.

Mottram (1993) came up with an innovative fabrication method of pGFRP close-sectioned beams and investigated the long-term properties of members assembled with the method. In his method, the pultruded beams were fabricated as an assembly of simple standard sections such as flat sheet and I-shape sections. These sections could be bonded by adhesive to compose a complex beam or column section, which improved the universality of the basic members. In a 24-hour creep test, a 22.8 kN mid-point load was applied to a 76 x 90 beam spanning 700 mm. The load represented the design load for the beam. Since the creep deflection was 10% of the initial deflection, the 24-hour tests were considered as an accelerated test and sufficient to predict the following creep behaviors. The Findley power law combined with Timoshenko beam theory was used for deflection prediction of one week, one year and ten years, which were estimated as 25%, 60% and 100% greater than initial deflection, respectively.

McClure and Mohammadi (1995) tested pGFRP angle stubs and corresponding coupons simultaneously under 2500-hour compressive load and proved the ability to predict long-term

behaviors of angle stubs through creep test results of corresponding coupons utilizing the Findley power law. In the creep test, both angles and coupons were loaded to 45% of their failure load. After 2500 hours, the average ratio of creep strain to initial strain was 14.4% for angle stubs and 13.8% for coupons. Although model parameters (E_t and n) determined from stubs and coupons were different, the authors reported good agreement between theoretical prediction and experimental results when attempting to predict strain-time curves of angle stubs based on coupon test results. For the parameter n, a difference was observed between angle stubs and coupons. An average value of 0.254 and 0.170 was obtained for angles and coupons, respectively, and no clear explanation for this difference was given in the article.

Scott and Zureick (1998) conducted compression creep tests on coupons from pGFRP I-beams for up to 10,000 hours. The results correlated well with predictions based on the Findley power law. Three stress levels were considered: 20%, 40% and 60% of the average compressive strength obtained from short-term tests. Specimens were loaded in a lever-arm creep fixture with concrete dead load and strain readings obtained over time. Using the test results, the first 1,000 hours were used to find the parameters of the Findley power law. The initial modulus was determined and the parameter $n = 0.23$ ($COV = 0.046$)was determined. Scott and Zureick found that the modulus parameter m varies considerably between specimens in each research program but the value of n for pGFRP is more consistent and almost the same as that reported by Mottram (1993). The scatter of parameter m could be explain by Equation 2.10 which showed that m varied with stress. Table 2.2 summarizes previous work based on the Findley power law and the parameters obtained from linear regression. The parameter m was converted into E_t to exhibit a unified parameter for each research work.

Table 2.2 Summary of previous work based on Findley power law

Authors	Creep Test	Specimen Type	E_t (GPa)	n
Mosallam and Bank (1991)	Flexural 2000 h	pGFRP frame	130	0.3
Mottram (1993)	Flexural 24 h	pGFRP beam flat sheet	590	0.22
	Flexural 24 h	pGFRP beam I-shape	500	0.21
McClure and Mohammadi (1995)	Compression 2500 h	pGFRP angle stub	520	0.17
	Compression 2500 h	pGFRP coupon	1150	0.25
Scott and Zureick (1998)	Compression 10,000 h	pGFRP column	1490	0.23
Kang (2001)	Flexural 8700 h	pGFRP beam	604	0.15

The variation of modulus should not be surprising. This value will reflect a large number of pGFRP geometric and material properties including a) fiber volume ratio; b) fiber architecture and pGFRP element thickness; and c) nature of the applied stress. The parameter *n*, on the other hand, is a measure of the viscoelastic response primarily of the resin. The resin properties of structural pGFRP do not vary nearly as much as the fibre volume and architecture.

2.4 SLENDER PGFRP COLUMN STABILITY

Hewson (1978) studied failure modes of channel-shaped pGFRP columns under axial compression. Nine types of specimens with different cross section size whose length ranged from 155 mm to 466 mm were tested and the results compared with predicted failure loads. The fixed-ended columns had slenderness ratios, *KL/r (*where *K* is the effective length factor, *L* is length and *r* is radius of gyration) ranging from 11.3 to 32.0 and were loaded to failure. The buckling load was obtained using Southwell's (1932) method. Southwell's method is a graphical method for non-destructive critical load determination of columns. Mid-height lateral deflection (δ) is plotted against the ratio of mid-height lateral deflection to applied load (δ/P). The slope ($\delta/(\delta/P)$) of the

resulting curve is an estimation of critical buckling load, P_{cr}. Failure modes considered were global (Euler) buckling, torsional buckling and local (flange) buckling. In the prediction, the author derived a non-dimensional graph which combined solutions of different failure modes to predict buckling loads of channel columns. The derivation was based on the assumption that isotropic theory using modified material properties could be used. The authors observed no local failure modes and reported that the experiments and predictions did not correlate well in terms of global buckling. The reason for the poor correlation was hypothesized to be imperfect load application and boundary conditions.

Barbero and Tomblin (1992) experimentally investigated global buckling of pGFRP I-shaped columns and validated the predictive capacity of Euler's equation:

$$P_E = \frac{\pi^2 E_L I_{min}}{(KL)^2} \tag{2.19}$$

In which E_L is the longitudinal elastic modulus, I_{min} is the weak-axis moment of inertia and KL is the column effective length. To address torsional buckling, an approximate analysis was conducted and the torsional buckling load was shown to be twice the Euler buckling load. Specimen slenderness, *KL/r* exceeded 95 and steel shoes were utilized at both ends to restrain torsion. The experimental buckling load was determined using Southwell's method, which required sufficient data and performed well for the single global buckling mode investigated. Pinned-pinned boundary conditions were used and loading progressed until midspan lateral deflection was L/100; this permitted sufficient data to be collected while maintaining the response in the linear range. The predicted Euler buckling load and experimentally observed buckling load differed by no more than 6% and predicted loads were generally higher than experimental loads. This variation is attributed to imperfections in specimens which are not considered in Equation 2.19.

Scott and Zureick (1997) performed a short-term buckling test of slender pGFRP columns with box and I-shaped cross sections and compared the experimental results with predictions based on Hewson's equations (Hewson 1978, Hewson and Lee 1979). Twenty-four specimens with lengths ranging from 1189 mm to 2444 mm and effective slenderness ratio, KL/r, ranging from 36 to 103 were included. Before testing, initial out-of-straightness was measured and checked against maximum tolerance limits of ASTM D3917-94 and material properties were determined. Longitudinal modulus and in-plane shear modulus was determined with tension tests, compression tests and asymmetric four-point bending tests on coupons which were cut from flanges and webs of the two types of columns. The modulus was observed to differ between web and flange coupons. In the buckling test, the load was applied at a constant rate until the deflection increased significantly. Deflection in both axial and lateral directions was measured during loading and the experimental buckling load was estimated using Southwell's method.

Critical load prediction was performed using buckling equations proposed by Hewson (Equation 2.20) which is a modification of the Euler buckling equation (Equation 2.19) accounting for the effects of shear.

$$P_e = \frac{P_E}{1 + \left(n_s P_E / A_g G_{LT}\right)} \tag{2.20}$$

In Equation 2.20, P_E is the Euler buckling load given by Eq. 2.19, A_g is the gross cross section area, n_s is the shape factor of shear, and G_{LT} is the in-plane shear modulus. The predicted loads based on Equation 2.20 were generally higher than corresponding experimental loads but still correlated reasonably well. The ratio of predicted load to experimental load ranged from 0.85 to 0.97 using Equation 2.19 and improved marginally to 0.88 to 1.01 using the correction for shear in Equation 2.20.

Due to the occurrence of several failure modes for columns of different size while under compressive load, Hashem and Yuan (2001) developed a criterion for pGFRP columns differentiating between short and long columns based on observed failure modes in experimental studies. Twenty-four pGFRP columns were tested to failure including "universal"-section columns with slenderness ratios (*KL/r*) ranging from 3.8 to 75.4 and box-section columns with slenderness ratios ranging from 9.4 to 78.9. Pinned-pinned boundary conditions were used and initial column position was adjusted using surveying levels – minimizing initial imperfections. In the accompanying analytical study, both Euler's formula (Equation 2.19) and classical Orthotropic Plate Theory (OPT) were utilized in failure load prediction. Experimentally, the division between short and long columns was determined at $KL/r = 50$. Analytically, equating the Euler equation to OPT, *KL/r* is found to be 46.6. The authors considered the difference to result from specimen and experimental setup imperfections. The conclusion was made that columns with slenderness ratios larger than 50 will fail in global elastic buckling. For such long columns, Euler's equation results in good predictions which were generally high but within 5% of the experimental results.

Bennett (2005) studied compressive creep behaviors of slender pGFRP square tube columns and proposed a semi-empirical expression to predict mid-height lateral deflection. In the experimental study, two environmental temperatures (23^{o}C and 65.5^{o}C) and three levels of concentric axial load (33%, 67% and 90% of short-term critical load, which was determined using Southwell's method) were included in the 1,000-hour tests. All columns were 1905 mm in length, 101.6 mm in width and 6.35 mm in wall thickness ($KL/r = 49.0$). Dial gages were utilized to measure lateral deflection, axial deflection and end rotation. The axial deflection was used for load lost estimation, which was about 3.8% of applied load during the test. Within the six specimens in different conditions, the one tested under 90% load and elevated temperature exhibited the largest

lateral creep deflection, 3.1 mm (L/614). In general, the lateral deflection increased with load and temperature. With the test results, the author modified the eccentric compressive creep buckling equation (Equation 2.21) proposed by Kang (2001) in terms of creep behavior and concentric loading and assumed a power law expression.

$$\delta = \sec\left(\frac{\pi}{2}\sqrt{\lambda} - 1\right) e + A_i \frac{\lambda}{1-\lambda} \tag{2.21}$$

$$\delta(\mathrm{t}) = A_i \frac{\lambda[1+\psi(t)]}{1-\lambda[1+\psi(t)]} \tag{2.22}$$

$$\psi(t) = \frac{t^n}{\beta} \tag{2.23}$$

In Equation 2.21, λ is the ratio of applied load to buckling load, e is eccentricity of applied load, A_i is the initial imperfection of the column which was determined from out-of-straightness tests based on *ASTM D3917 Standard Specification for Dimensional Tolerance of Thermosetting Glass-Reinforced Plastic Pultruded Shapes*. In Equation 2.23, β and n were determined from the long-term deflection data. In the comparison between prediction and experimental results, parameters could be found that resulted in good agreement for most specimens although the parameters obtained for columns under different test conditions (load levels and temperature) were not consistent, suggesting that these parameters are functions of both load and temperature.

Besides Equation 2.21 proposed by Bennett (2005), there is another expression based on viscoelasticity theory to describe time-dependent lateral deflection during creep buckling of viscoelastic columns, which was described by Bazant (2010). For slender elastic columns, the differential equation describing short-term stability is

$$(v'' - v_0'') + \frac{P}{EI} v = \frac{M_0}{EI} \tag{2.24}$$

where $v_0(x)$ is the initial curvature which is inevitable in practice and M_0 is the moment caused by lateral force. For typical column behavior, no lateral load is present, therefore Equation 2.24 may be written as:

$$EI(v'' - v_0'') + Pv = 0 \tag{2.25}$$

When it comes to time-dependent buckling of pGFRP columns, the viscoelasticity of the material must be considered. Based on the Kelvin standard solid model, Bazant proposed the partial differential equation (Equation 2.26) in space and time governing creep buckling of a pinned-pinned viscoelastic column can be derived by replacing E with differential operator $\underline{E}$ (Equation 2.27). The differential operator was defined in Equation 2.28, which relates long-term strain and stress in differential form.

$$v'' - v_0'' + \tau_r \dot{v}'' + \frac{P}{E_\infty I} v + \frac{P}{E_0 I} \tau_r \dot{v} = 0 \tag{2.26}$$

$$\underline{E} = \frac{1 + \tau_r(\frac{\partial}{\partial t})}{\left(\frac{1}{E_\infty}\right) + (\frac{\tau_r}{E_0})(\frac{\partial}{\partial t})} \tag{2.27}$$

$$\sigma = \underline{E}\varepsilon \quad \text{or} \quad \varepsilon = \underline{E}^{-1}\sigma \tag{2.28}$$

Equation 2.26 can be solved in the simplified form of Equation 2.29 in which $f^K(t)$ is the deflection ratio satisfying the boundary conditions of pinned-end columns and initial imperfection when $f^K = 1$. The sine function in Equation 2.29 made it possible to obtain lateral deflection at any height, $\underline{x}$, of the column. Equation 2.30 is the initial condition ($t = 0$) of function $f^K(t)$, which was obtained by multiplying with magnification factor μ (Equation 2.31).

$$v = f^K(t) A_i \sin\frac{\pi x}{l} \tag{2.29}$$

$$f^K = \frac{1}{1 - P/P_{E_0}} \tag{2.30}$$

$$\mu = \frac{1}{1 - P/P_{cr}} \tag{2.31}$$

Substituting Equation 2.29 into Equation 2.26 and combining the initial condition of function $f^K(t)$, the expression of $f^K(t)$ can be derived as:

$$f^K(t) = \frac{1}{1 - P/P_{E_\infty}}\left(1 - e^{-\frac{t}{\tau_b}}\right) + \frac{1}{1 - P/P_{E_0}} e^{-\frac{t}{\tau_b}} \tag{2.32}$$

in which

$P_{E_\infty} = \pi^2 E_\infty I/L^2$,

$P_{E_0} = \pi^2 EI/L^2$, and

$\tau_b = \tau_r \frac{1-P/P_{E_0}}{1-P/P_{E_\infty}}$.

Retardation time, τ_r, is defined in relation to Equation 2.17. Based Equation 2.32, Bazant also provides typical deflection ratio curves (Figure 2.4). The three types of function shape result from the load being less than, equal to or greater than P_{E_∞}.

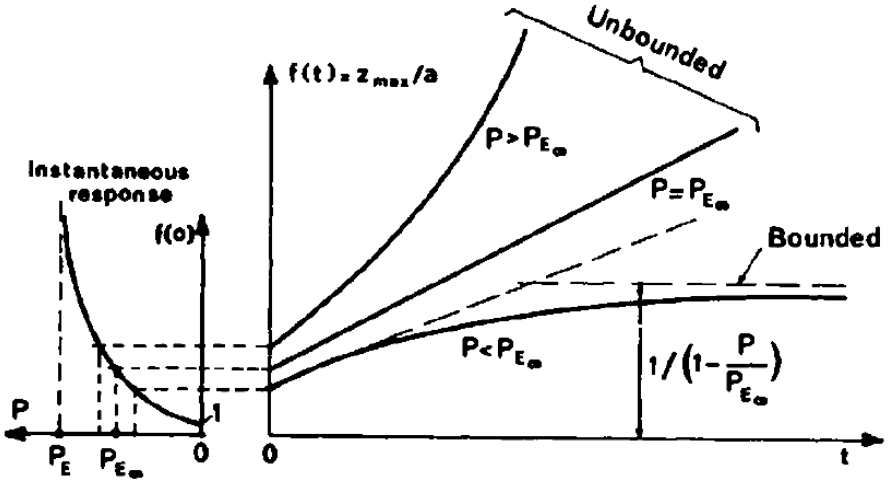

Figure 2.4 Deflection ratio curve in different conditions (Bazant 2010)

2.5 SUMMARY

In this chapter, the Findley power law has been shown in many research works to be reliable to describe flexural creep behaviors and make long-term predictions of pGFRP composites although empirically derived parameters must be established. For short-term stability investigation, Southwell's method has been widely and successfully used to determine critical buckling load of pGFRP columns. Only the research work of Bennett (2005), however, addressed creep buckling of slender pGFRP columns under concentric loading. Bennet's work focused on the influence of elevated temperature and load levels on the time-dependent lateral deflection curve derived based on an eccentric creep buckling expression proposed by Kang (2001). The theoretical prediction based on the expression was observed to be less consistent with experimental results at higher load levels. Besides Bennett's theoretical model, Bazant also proposed an equation to predict the time-dependent lateral deflection curve based on an analytical derivation of viscoelastic theory. No experimental investigation has been conducted to investigate the critical time of creep buckling in slender pGFRP columns. Thus the predictive capacity of Bazant's equation was not tested.

3.0 FLEXURAL CREEP TESTS

In this chapter, the experimental investigation of flexural creep behavior of pGFRP plate specimens is presented. Short-term tests were conducted to determine initial modulus and strength of the material. In the creep tests, six specimens under three levels of stress are loaded for more than 1,000 hours to obtain long-term flexural behaviors. Using strain history data, the modulus required for the Kelvin standard solid model and Findley power law are determined through curve fitting. The experimentally established parameters can be used to predict creep buckling behaviors of pGFRP as described in Chapter 4.

3.1 SHORT-TERM MATERIAL PROPERTIES

All specimens reported in this work are cut from pGFRP plate having nominal thickness of 6.4 mm. Typical specimens, shown in Figure 3.1, were nominally 38 mm wide. The plate architecture contained three layers of unidirectional glass fiber separated by four layers of continuous strand mat and two surfacing veils in an isophthalic polyester resin matrix. Manufacturer reported and experimentally obtained material properties are given in Table 3.1. Longitudinal and transverse properties of the material were determined in an earlier study (Harries and Cunningham 2015).

Table 3.1 Material properties of 6.4 mm thick pGFRP plate

Property	Manufacturer reported (Bedford Reinforced Plastics 2012)	Experimentally determined (COV in brackets)
Longitudinal modulus determined from tension test, E_{Lt}	13.8 GPa	19.9 GPa[a] (0.04)
Longitudinal strength determined from tension test, F_{Lt}	165 MPa	425 MPa[a] (0.06)
Tranverse modulus determined from tension test, E_{Tt}	7600 MPa	6400 MPa[a] (0.07)
Transverse strength determined from tension test, F_{Tt}	69 MPa	94 MPa[a] (0.04)
Longitudinal modulus determined from flexure test, E_{Lf}	13.8 GPa	19.9 GPa (0.02)
[a] Harries and Cunningham 2015		

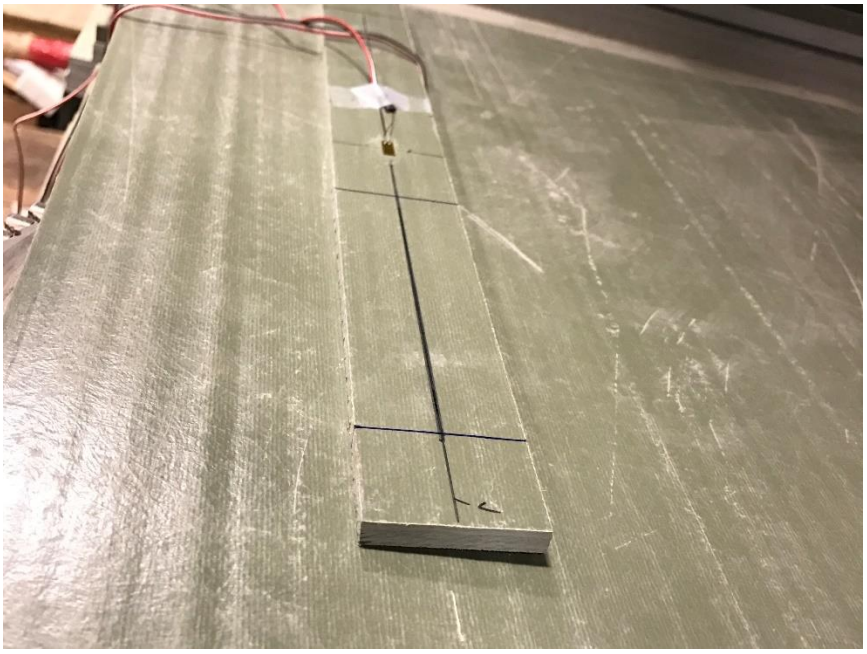

Figure 3.1 38 x 6.4 mm pGFRP flexural specimen

In this work, short-term longitudinal modulus was determined in a flexural test. Three 38 mm wide beams cut from the 6.4 mm pGFRP plate were loaded in the same flexural configuration as used for the creep tests (described below). Loads were incremented in 90 N steps up to about

one-half the flexural capacity of the beams. Both tensile and compressive strain were recorded for determining longitudinal modulus which, as shown in Table 3.1, was found to be the same as that determined previously using tension tests: 19,900 MPa. Figure 3.2 shows data from a representative specimen in which the strain-stress relationship for both tension and compression strains are essentially linear. A small apparent in shift in the neutral axis of about 1.6% the specimen depth toward the compression face is seen in Figure 3.2. This is believed to reflect variation in the fiber architecture in the specimen.

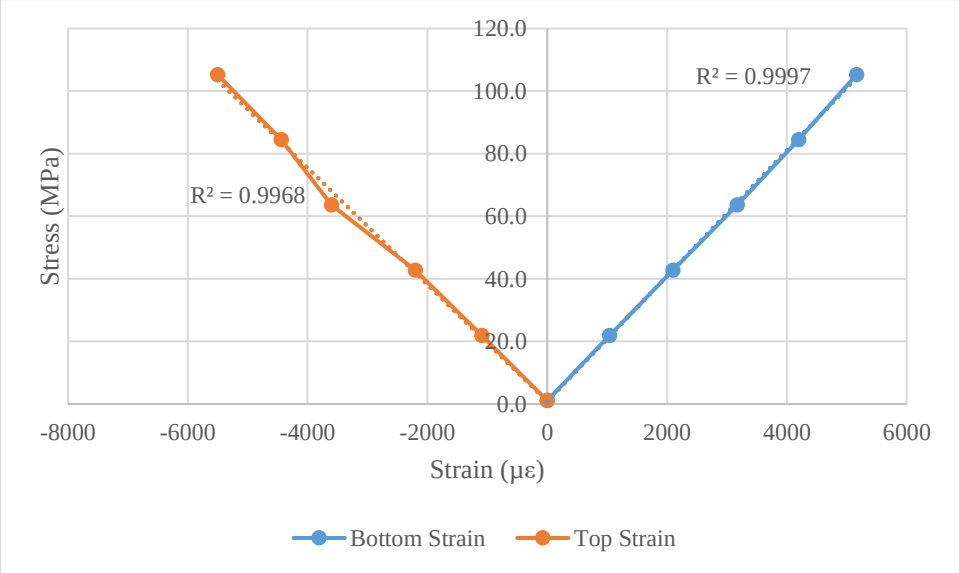

Figure 3.2 Representative stress strain curve from flexural test

3.1.1 Test setup

A four-point bending test set-up is used as shown in Figure 3.3. Specimens are loaded with free weights (Figure 3.4) through a channel spanning the constant moment region. The loading channels have rounded edges with a radius of 2.5 mm (0.10 inch) so as to not damage the pGFRP.

Each beam is supported over a 304.5 mm clear span on 12.7 mm diameter steel rollers. The support span-to-depth ratio is about 48 and shear span-to-depth ratio is about 18, which are consistent with requirements of ASTM D6272-10 *Standard Test Method for Flexural Properties of Unreinforced and Reinforced Plastics and Electrical Insulating Materials by Four-Point Bending.* This slender specimen geometry minimizes the effects of shear. The assembly weight including the loading channel and free-weight support assembly was 4.67 N which is added to all applied loads. The entire assembly is mounted on steel grid deck allowing steel wires to transfer loads from free weight below the grates.

Stress in the extreme fibers of the specimen in four-point flexure was calculated as follows:

$$\sigma = \frac{My}{I} = \frac{\mathrm{Pa}}{2}\left(\frac{d}{2}\right)\left(\frac{12}{bd^3}\right) \qquad (3.1)$$

in which b is measured specimen width and d is the measured thickness; $M = \frac{\mathrm{Pa}}{2}$ is the applied moment; P is the total applied load and a is the shear span, which is 116.8 mm as shown in Figure 3.3; y is the position of specimen neutral axis determined from top and bottom surface strain data; and, $I = \frac{bd^3}{12}$ is moment of inertia of the specimen cross section.

Strain gauges (seen in Figure 3.1) were attached on both top and bottom surfaces at the mid-span of the beam to measure the maximum of tensile and compressive strains (from which the neutral axis may be calculated). Strains were recorded at predetermined intervals using a P3 strain indicator (Figure 3.5). Vertical deflection at mid-span was also tracked utilizing a digital micrometer depth gauge (Figure 3.5) with the steel grid deck functioning as reference.

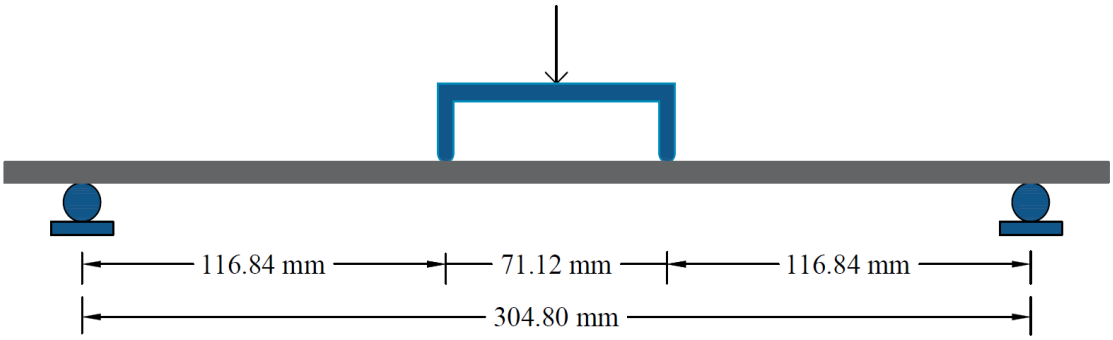

Figure 3.3 Four-point flexure test configuration

Figure 3.4 Creep test configuration showing four specimens under loads of 445 and 667 N

Figure 3.5 P3 strain indicator and depth gauge

3.1.2 Test protocol

Three stress levels were achieved in the creep test. Based on ASTM D2990-09 *Standard Test Methods for Tensile, Compressive, and Flexural Creep and Creep-Rupture of Plastics*, the three stress levels were proposed to be 0.12, 0.24 and 0.37 of the failure load. Free weights used in each case were 50 lbs (222N) for specimens A/B, 100 lbs (445 N) for specimens C/D and 150 lbs (667 N) for specimens E/F. Initial loading of specimens was rapid (less than 15 seconds to avoid creep before initial readings) and smooth to avoid vibration and impact. The stress levels were selected to keep the creep process in its primary stage (Figure 2.1) which exhibits linear viscoelasticity. Measured specimen dimensions, total applied creep load and neutral axis location based on initial strain data are provided in Table 3.2. Considering the slight difference in specimen dimension, the ratios of applied load to failure load were marginally different than targeted as shown in Table 3.2. The neutral axis location is defined as a portion of specimen depth measured from the extreme tension face. Thus a value greater than $\alpha = 0.50$ indicates a shift of the axis toward the compression face.

Table 3.2 Flexural specimen dimension and load

Specimens	Width b (mm)	Thickness d (mm)	Neutral Axis α[1]	Applied Load P (N)	Load to P_{ult} ratio
FLX_C_A	38.99	6.26	0.51	227	0.12
FLX_C_B	39.05	6.17	0.48	227	0.13
FLX_C_C	38.74	6.19	0.50	450	0.25
FLX_C_D	38.83	6.21	0.50	450	0.25
FLX_C_E	38.69	6.16	0.52	672	0.38
FLX_C_F	38.83	6.15	0.51	672	0.38

[1] based on initial strains upon loading

Strain and deflection readings were taken at the following intervals:

- immediately following loading (short-term properties);
- 15 minute intervals for the first five hours;
- 30 minute intervals from 5 to 11 hours;
- 6 hour intervals for the following 96 hours; and
- 24 hour intervals for the duration of the test (>1000h)

During the creep test, the ambient environmental conditions were essentially constant as required by ASTM D2990-09. The temperature remained at 21±1 ^{o}C and average relative humidity was 53±5%.

3.2 EXPERIMENTAL RESULTS

3.2.1 Deflection and strain

The test results for mid-span strain and deflection are presented in Tables 3.3 and 3.4, respectively. Corresponding strain and deflection time histories are shown in Figures 3.6 and Figure 3.7, respectively. In Figure 3.6, only the creep strain is shown (strain following initial loading). Creepocity (the ratio of creep strain to initial strain) is expressed as:

$$\text{creepocity} = \frac{\varepsilon(t) - \varepsilon_0}{\varepsilon_0} \tag{3.2}$$

where $\varepsilon(t)$ is the strain reading at time t and ε_0 is the strain upon loading. In all six specimens, strain increased with time at both top and bottom surfaces. Bottom strain (tensile) generally increased more than top strain (compressive), resulting in a downward shift of neutral axis.

Although absolute strains were proportional to the load level (as expected), the creepocity after 1000 h was similar for all specimens with no clear trend established based on load level.

As described in Section 2.1, there are three stages in creep process of pGFRP materials. In the primary stage, creep begins rapidly and becomes slower with time. In the secondary, or steady state, stage, creep rate is almost zero. Finally in the tertiary stage, accelerating creep rates occur leading to material failure. The length of these stages is a function of the load level. In this test, specimens A/B, under the lowest load, showed the shortest primary stage (less than 24h), and appeared to enter the secondary phase in which creep rate becomes negligible. The more heavily loaded specimens remained in the primary stage longer and in proportion to their load level: the primary stage of specimens C/D was about 200h while that for E/F was a bit longer (Figure 3.6).

Table 3.3 Flexural creep test results of strain

Specimens	Stress (MPa)	Strain upon Loading (με)		1000-h Strain (με)		1000-h Creepocity	
		Bottom	Top	Bottom	Top	Bottom	Top
FLX_C_A	52	3036	-2958	3438	-3258	0.13	0.10
FLX_C_B	54	2202	-2375	2531	-2724	0.15	0.15
FLX_C_C	106	5308	-5242	6191	-6030	0.17	0.15
FLX_C_D	105	5451	-5520	6446	-6556	0.18	0.19
FLX_C_E	160	7786	-7195	8938	-8085	0.15	0.12
FLX_C_F	160	8178	-7929	9305	-9038	0.14	0.14

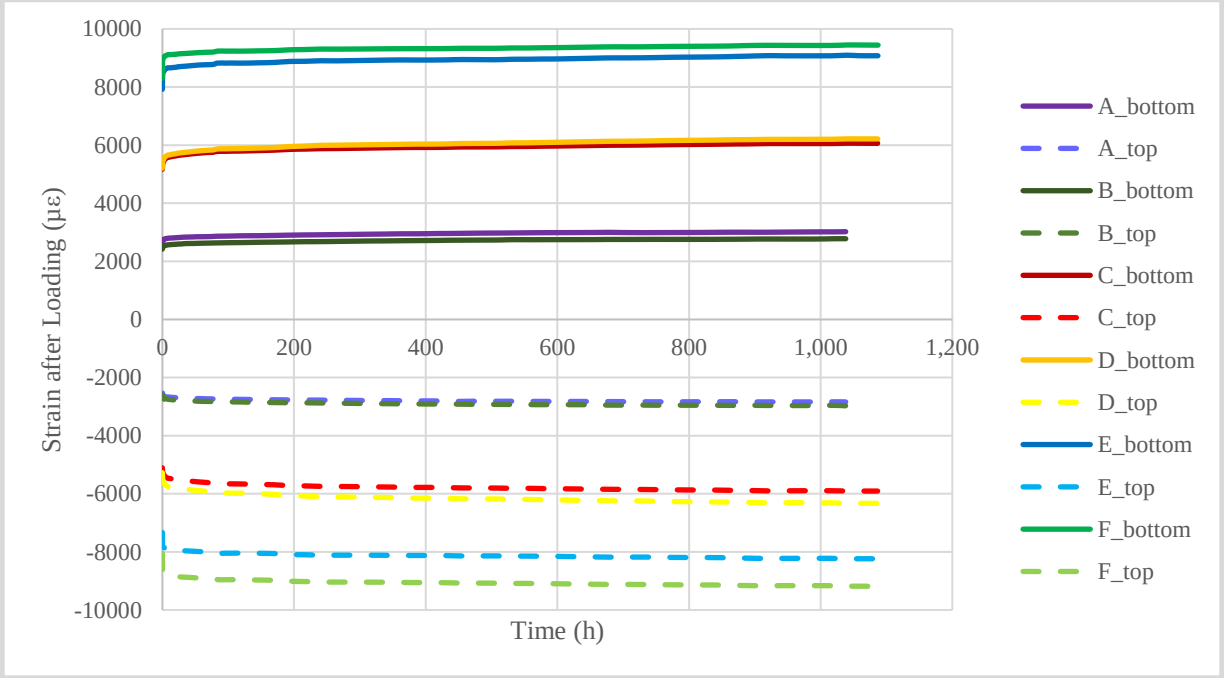

Figure 3.6 Flexural strain-time curve after loading

Table 3.4 Flexural creep test results of deflection

Specimens	Stress (MPa)	Initial Deflection (mm)	1000 h Deflection (mm)	1000-h Deflection Increase (mm)	
FLX_C_A	52	8.32	9.87	1.55	18.6%
FLX_C_B	54	8.60	10.29	1.69	19.7%
FLX_C_C	106	14.68	17.05	2.37	16.1%
FLX_C_D	105	14.01	16.99	2.98	21.3%
FLX_C_E	160	22.34	25.57	3.23	14.5%
FLX_C_F	160	24.05	27.62	3.57	14.8%

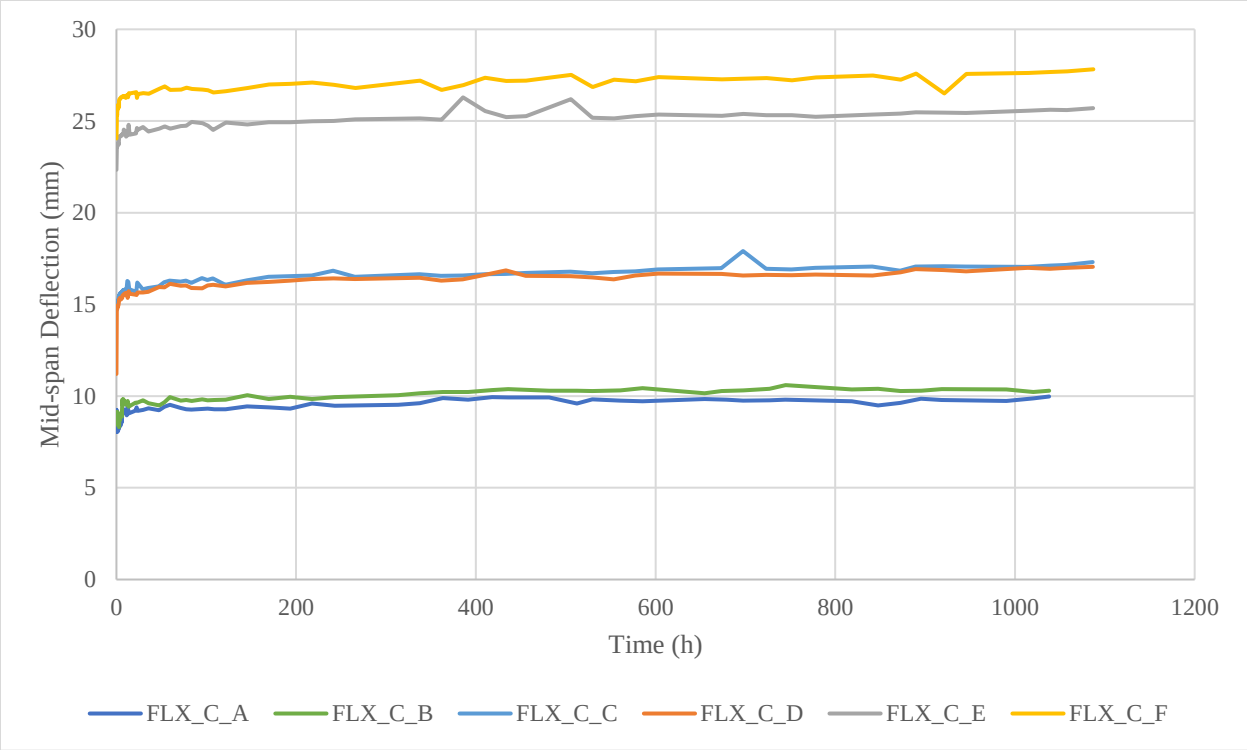

Figure 3.7 Flexural deflection-time curve after loading

3.2.2 Young's modulus

Table 3.5 presents longitudinal moduli calculated from the initial loading and after 1000 h. The initial longitudinal modulus, E_0 = 20.9 GPa, slightly greater than that determined from earlier material characterization tests (Section 3.1). The reason for this discrepancy is not clear although the variation in fiber architecture from specimen to specimen is known to affect this value significantly (a separate study is currently underway to quantify this effect for the materials tested; variation on the order of 10-15% has been observed). After 1000 h under load, the apparent modulus based on measured strains is 17.7 GPa, a decrease of about 16%.

Table 3.5 Initial and 1000-h longitudinal modulus

Specimens	Stress (MPa)	E_0 (GPa)	E_{0_avg} (GPa)	COV	E_{1000_bottom} (GPa)	E_{1000_top} (GPa)	E_{1000_avg} (GPa)	COV
FLX_C_A	52	21.1	20.9	0.022	15.2	16.0	17.7	0.096
FLX_C_B	54	21.5			21.2	19.7		
FLX_C_C	106	21.1			17.2	17.6		
FLX_C_D	105	20.5			16.3	16.1		
FLX_C_E	160	21.2			17.9	19.8		
FLX_C_F	160	20.1			17.2	17.7		

3.2.3 Neutral axis shift

As shown in Table 3.6, only a very slight shift of neutral axis was observed during the creep tests. Although there was no clear trend, the initial neutral axis was observed to be shifted toward the compression face (top) of the specimen in 4 of the 6 specimens, In each of these specimens, the neutral axis shifted very marginally further toward to the compressive face. This resulted in a subtle asymmetric behavior of the compressive and tensile zones.

Because the load levels were relatively low, and the creep behavior remained in the primary and secondary phases, little shift in neutral axis is expected. The viscoelastic behavior of pGFRP in these phases of behavior is typically assumed to be linear; thus tension and compression behavior should be symmetric.

Table 3.6 Flexural test results of neutral axis location

Specimens	Stress (MPa)	Initial Neutral Axis, α	1000-h Neutral Axis, α	Shift of Neutral Axis (mm)
FLX_C_A	52	0.507	0.513	+0.04
FLX_C_B	54	0.481	0.482	+0.00
FLX_C_C	106	0.503	0.507	+0.02
FLX_C_D	105	0.497	0.496	-0.01
FLX_C_E	160	0.520	0.525	+0.03
FLX_C_F	160	0.508	0.507	-0.00

3.3 ANALYSIS AND DISCUSSION

Experimental results are further discussed in this section. Modulus determination for both the Kelvin standard solid model and Findley power law is presented. A curve fitting program based on the concept of enumeration written in MATLAB was utilized to find the parameters, τ_r and E_∞ for the Kelvin Model and n and E_t for Findley power law. The resulting predictive capacities of the two models is presented.

3.3.1 Kelvin standard solid model

In this work, the time-dependent constitutive equation derived from the Kelvin standard solid model was expressed as (see Section 2.1.2, Equation 2.19).

$$\frac{\varepsilon(\mathrm{t})}{\sigma} = \frac{1}{\mathrm{E(t)}} = [\frac{1}{E_\infty} - \left(\frac{1}{E_\infty} - \frac{1}{E_0}\right) * e^{-\frac{t}{\tau_r}}] \tag{3.3}$$

where E_0 is the initial longitudinal modulus, E_∞ is the long term (infinite) longitudinal modulus, t is time under load and τ_r is the retardation time, which is a time describing the response of a

viscoelastic material to the instantaneous application of a constant stress. As is observed in Equation 3.3, $\varepsilon(t) \rightarrow \sigma/E_0$ when $t \rightarrow 0$ and $\varepsilon(t) \rightarrow \sigma/E_\infty$ when $t \rightarrow \infty$. τ_r and E_∞ are the parameters in the Kelvin Model that need to be determined.

Using a MATLAB script (Appendix A.1), the approximate range of τ_r and E_∞ was set as 1-100 hours (1 hour increments) for τ_r and 15-21 GPa (0.1 GPa increments) for E_∞. Then the moduli were assigned values from the lower bound of the range to the upper bound and combined to estimate the experimentally determined strain values. In order to find the best combination of parameters, the least square method was utilized to quantify the curve fitting effect. For every combination of τ_r and E_∞, the square of the difference between predicted and experimental strain was summed and lowest least square result was selected as the best fit. Considering the reducing density of test data with time, the difference square in the first few days was given greater weight in the sum compared to the remainder of the test. Since approximately 40 strain readings were taken in the first day and subsequently reduced to once per day, a weight factor of 40 was included to balance the nonuniform data density. The resulting combination of parameters which led to the best fit for each test are summarized in Table 3.7. The sum of squares of difference was normalized by 1E+06 in both Kelvin model and Findley for clarity.

Table 3.7 Kelvin model modulus determination by enumeration (COV in brackets)

Specimens	Stress (MPa)	1000-h E Experimental	Goodness of fit (normalized sum of squares of difference)	Predicted E_∞ (GPa)	Average E_∞ (GPa)	τ_r (hours)	Average τ_r (hours)
FLX_C_A	52	17.7 (0.096)	0.8	18.4	18.0 (0.048)	54	61 (0.069)
FLX_C_B	54		1.3	18.3		63	
FLX_C_C	106		3.5	17.9		63	
FLX_C_D	105		8.2	16.7		68	
FLX_C_E	160		3.0	19.5		60	
FLX_C_F	160		20.0	17.5		60	

As shown in Table 3.7, the 1000-h longitudinal modulus determined through test results was 17.7 GPa and the predicted infinite modulus was 18.0 GPa with COV of 5%. The predicted long term modulus, E_∞, was higher than the experimentally determined 1000-hour modulus due to the inadequate capacity of Kelvin model to fully capture the creep behavior of pGFRP materials. As observed in Figure 3.8, the curves obtained for the Kelvin model fail to capture the initial high rate of creep and became very flat (secondary creep phase) after the retardation time.

3.3.2 Findley power law

The constitutive equation of pGFRP and its derivation based on the Findley power law has been presented in Chapter 2.1.1. In this section, Equations 3.4-3.6 are utilized for curve fitting and modulus determination based on the experimentally obtained data.

$$\varepsilon = \varepsilon_0 + mt^n \tag{3.4}$$

$$\log(\varepsilon - \varepsilon_0) = n \log t + \log m \tag{3.5}$$

$$\varepsilon = \sigma\left(\frac{1}{E_0} + \frac{t^n}{E_t}\right) = \frac{\sigma}{E(t)} \tag{3.6}$$

Equation 3.4 has been widely used by previous authors and is usually derived to the form of Equation 3.5. This derivation changes the power relationship to a linear relationship, which makes the modulus determination a more direct process (Appendix B). In this work, the moduli m and n obtained using Equation 3.5 are given in Table 3.8.

Table 3.8 Findley power law modulus determination with Equation 3.5

Specimens	Stress (MPa)	n	m	coefficient of determination, R^2
FLX_C_A	52	0.176	92	0.9977
FLX_C_B	54	0.184	105	0.9935
FLX_C_C	106	0.187	224	0.9836
FLX_C_D	105	0.178	304	0.9927
FLX_C_E	160	0.084	488	0.9840
FLX_C_F	160	0.076	643	0.9889

The values of n_F were consistent for specimens A/B/C/D, resulting in an average n_F of 0.181 with COV of 0.026. But for specimens E/F, n was smaller. This inconsistency could be explained by the range of applicability of the Findley power law. In the derivation of Findley power law in Section 2.2.1, Equation 3.4 is valid when the applied load is low compared to the failure load (Horvath, 1998). Since specimens E/F were subject to 38% of their failure load, Equation 3.4 may not be appropriate to characterize creep behaviors under this higher stress level. Modulus m varied with the three different stress levels tested. The difference between 1000-hour strain and strain upon loading increased with stress levels. Thus, it is reasonable that m also varied with load, considering the relationship of Equation 3.4.

In addition to the analytical method derived from the power law, the enumeration method used for the Kelvin model was also used for the Findley power law (Equation 3.6 and Appendix

A.2) and the resulting moduli are presented in Table 3.9. 100-700 GPa was set as range of E_t with an interval of 10 GPa and 0.01-0.30 was set for n with an interval of 0.01.

Table 3.9 Findley power law modulus determination with Equation 3.6

Specimens	Stress (MPa)	Goodness of fit (normalized sum of squares of difference)	E_t (GPa)	n
FLX_C_A	52	0.01	340	0.13
FLX_C_B	54	0.03	330	0.15
FLX_C_C	106	0.03	370	0.16
FLX_C_D	105	0.07	250	0.15
FLX_C_E	160	0.08	630	0.14
FLX_C_F	160	0.08	230	0.08

Assuming specimens E/F were not appropriate for the application of Findley power law and only considering the four specimens under lower loads, the average E_t was 322 GPa (COV of 0.138) and the average n was 0.15 (COV of 0.078).

3.3.3 Comparison and discussion

Figure 3.8 – 3.14 showed the comparison between experimental results and three series of theoretical results provided by Kelvin model (enumeration method), Findley model (analytical method) and Findley model (enumeration method). Generally, the Findley power law provides a better curve shape compared with the Kelvin standard solid model. In the Kelvin model, the strain increased rapidly before the retardation time and became rather constant after that. This property made it hard to predict the short-term creep of pGFRP materials, in which most specimens were in their primary stage of creep and showed high creep rates. But when the creep strain grew slowly

and transitioned into the secondary stage, the prediction of the Kelvin Model would be more consistent with experimental results. As for Findley power law, it showed high level of fitting from the beginning to the end of the creep test. For the two methods based on the Findley model, the enumeration method provided better consistency with test results as compared to the logarithmic method.

Figure 3.14 – 3.19 showed the modulus reduction in pGFRP creep behaviors, which corresponds to the creep deformation behaviors. Similar to Figure 3.8 – 3.13, experimental results and three series of theoretical prediction are shown. As indicated in Figure 3.14 – 3.19, the modulus predicted by the Kelvin model approached a constant value while the modulus predicted by the Findley model kept declining.

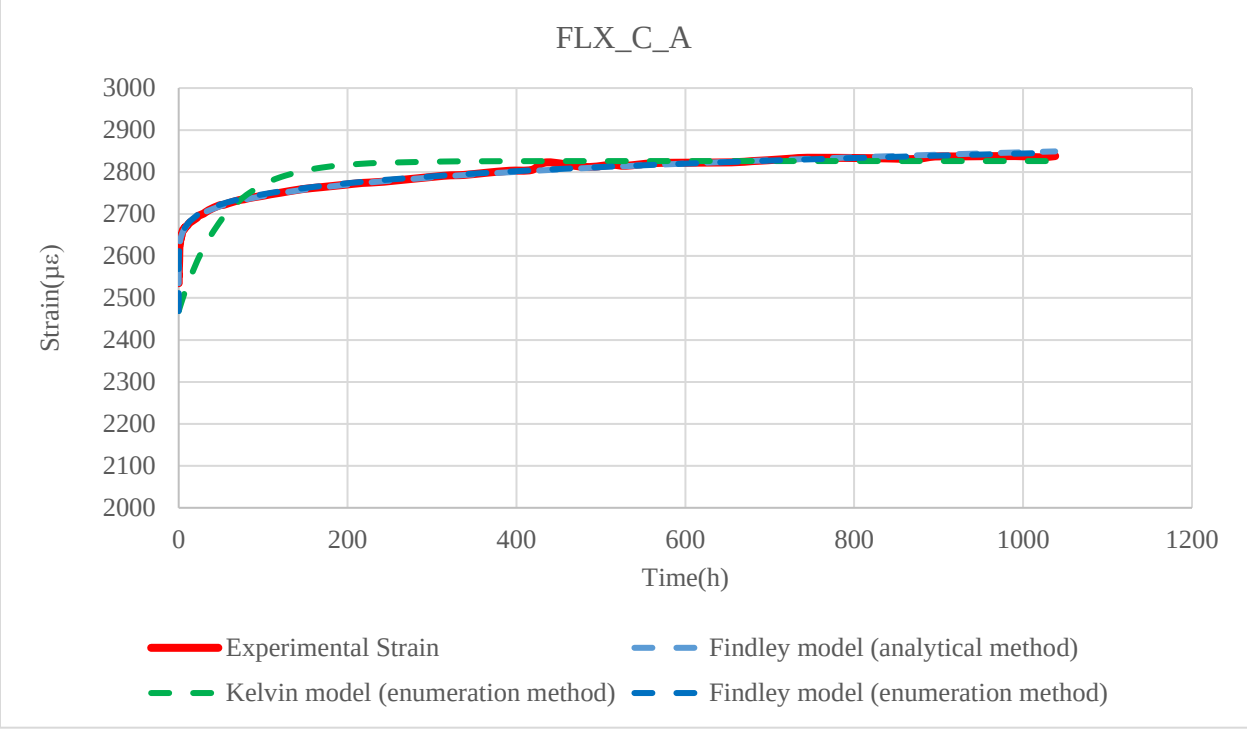

Figure 3.8 Comparison of theoretical and predicted strain results of FLX_C_A

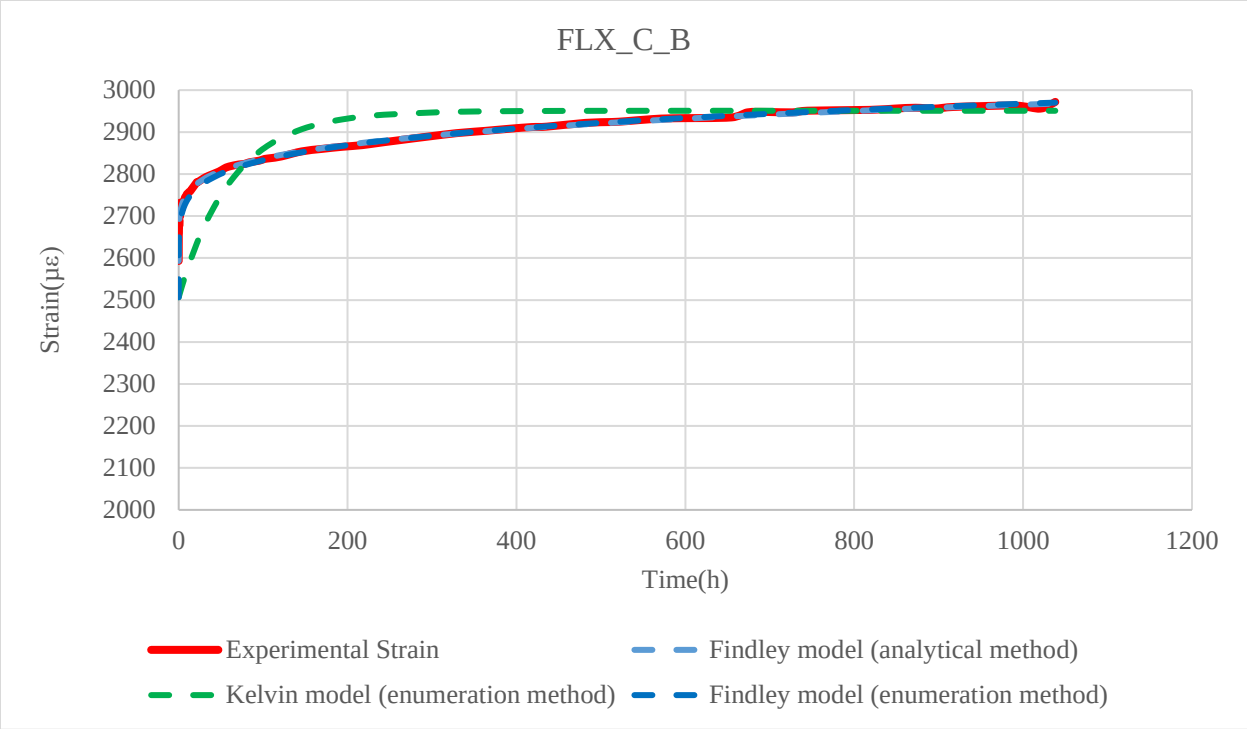

Figure 3.9 Comparison of theoretical and predicted strain results of FLX_C_B

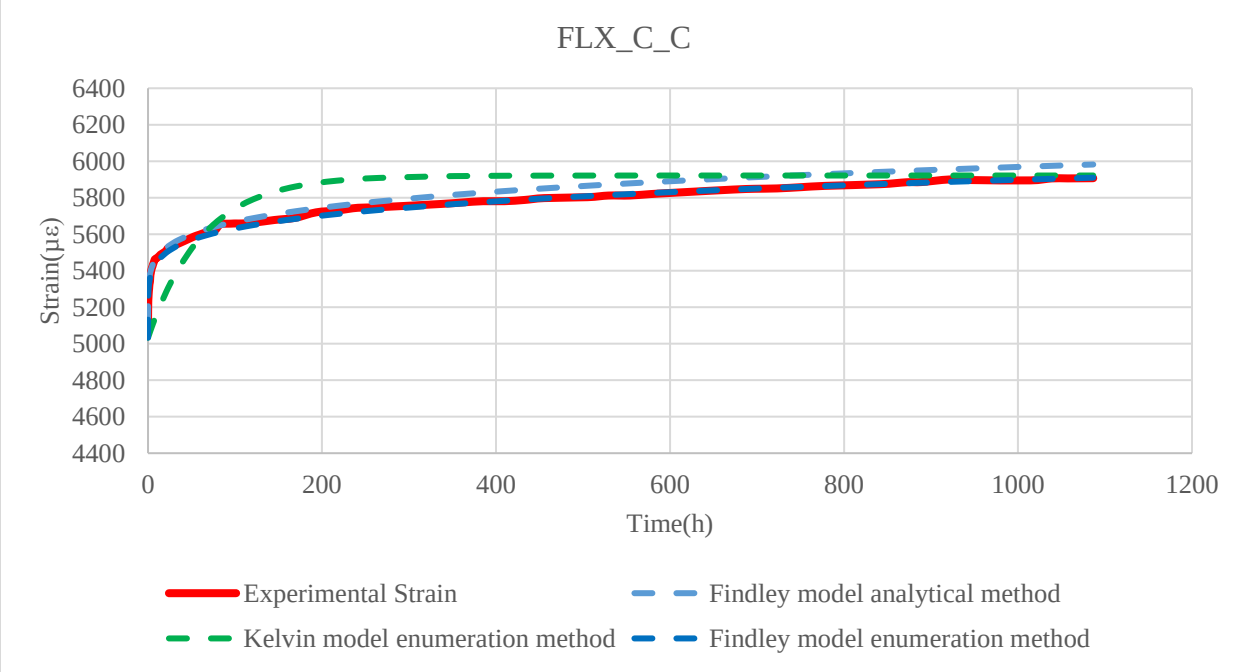

Figure 3.10 Comparison of theoretical and predicted strain results of FLX_C_C

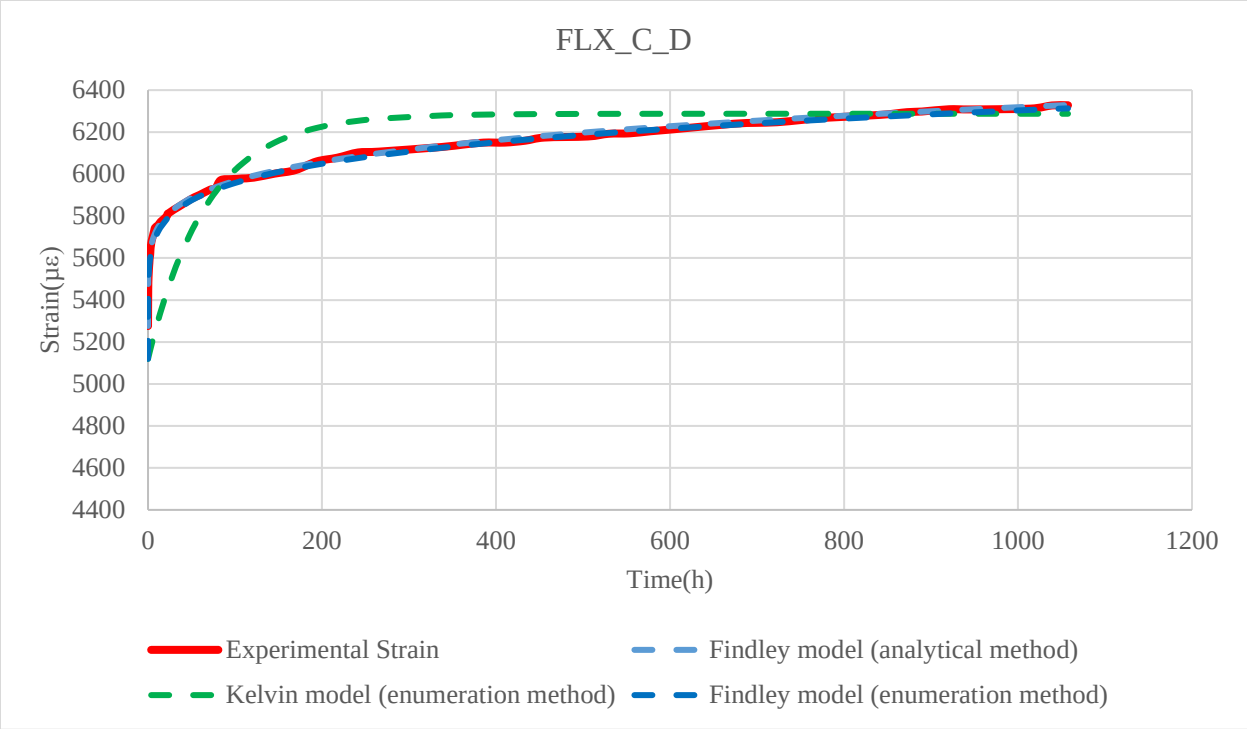

Figure 3.11 Comparison of theoretical and predicted strain results of FLX_C_D

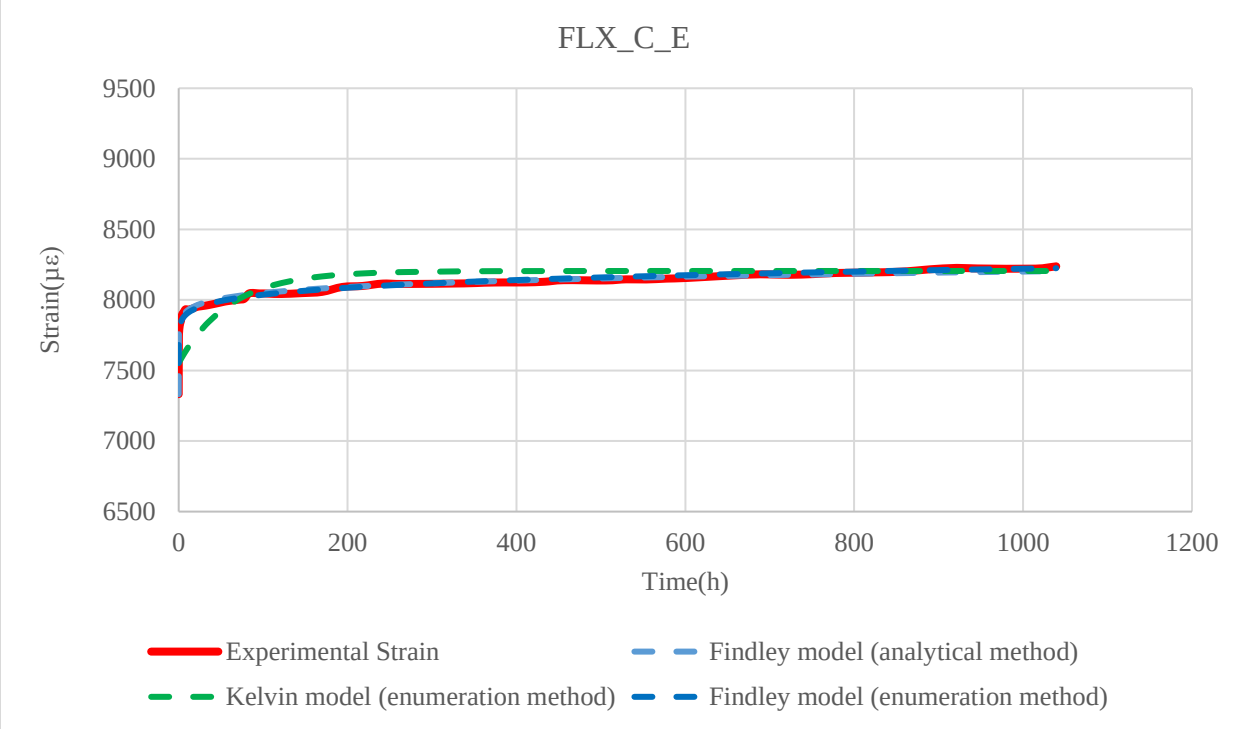

Figure 3.12 Comparison of theoretical and predicted strain results of FLX_C_E

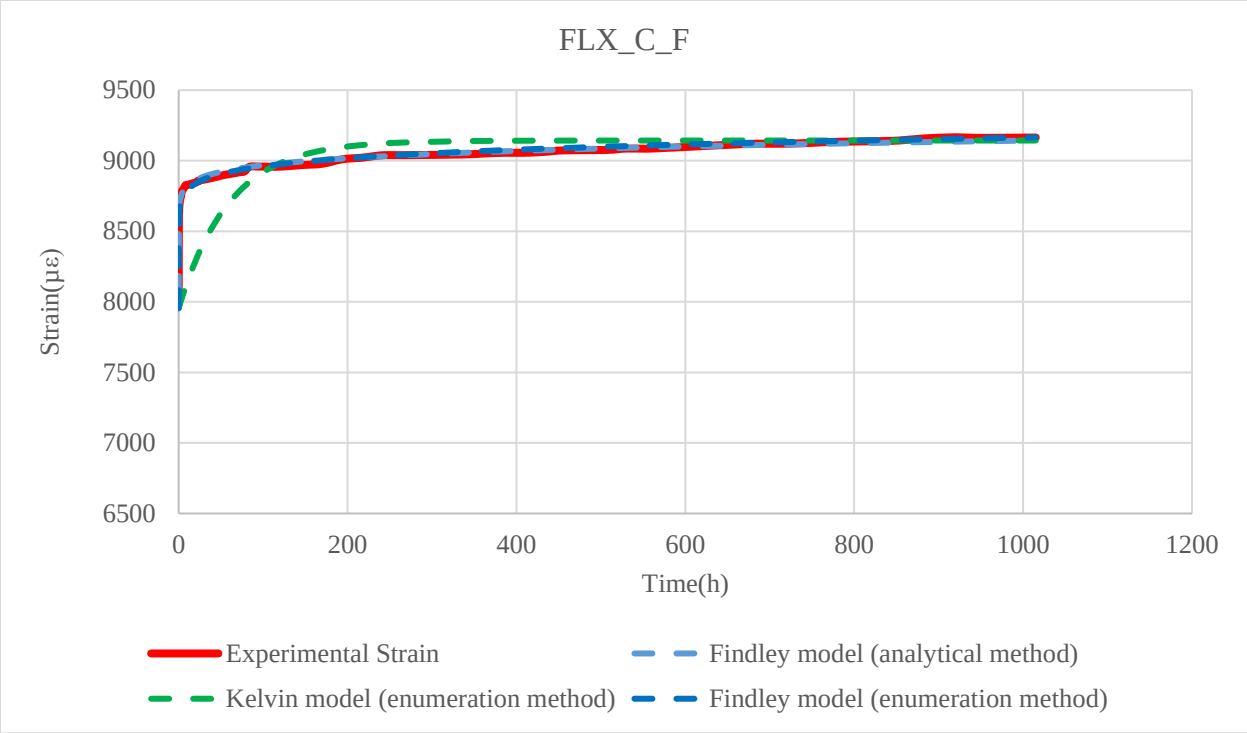

Figure 3.13 Comparison of theoretical and predicted strain results of FLX_C_F

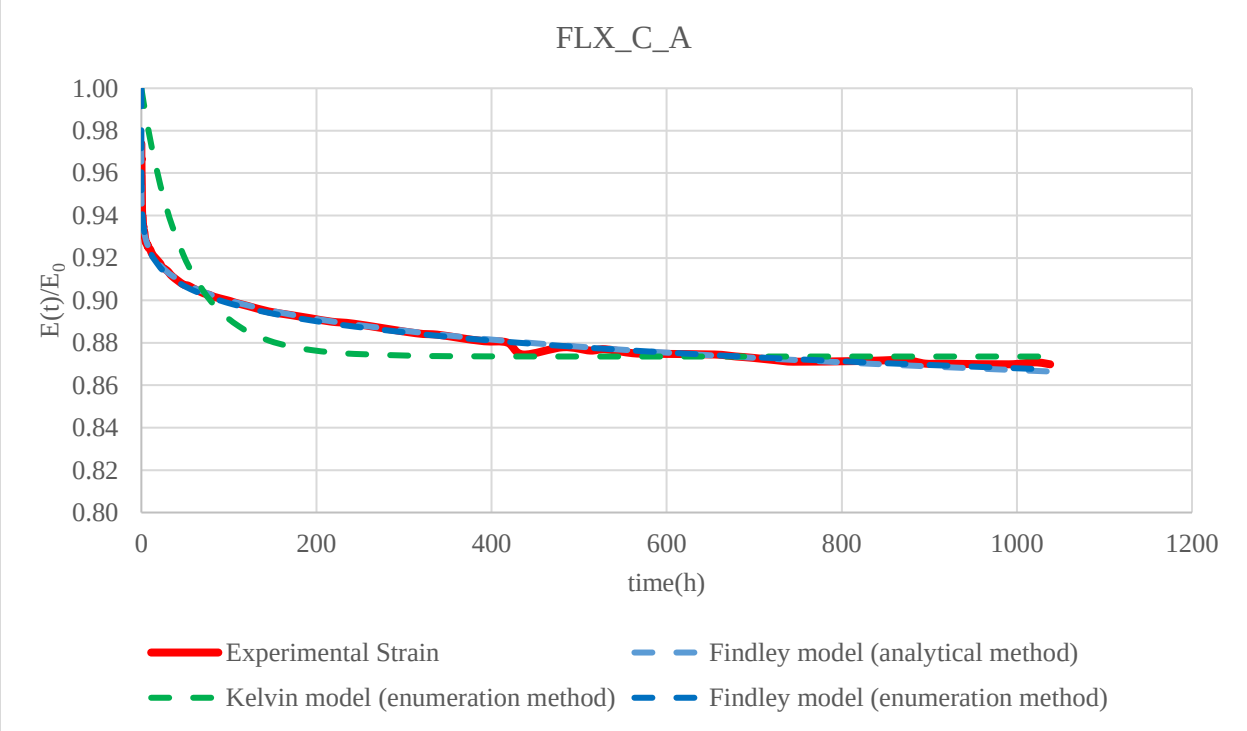

Figure 3.14 Comparison of theoretical and predicted modulus reduction of FLX_C_A

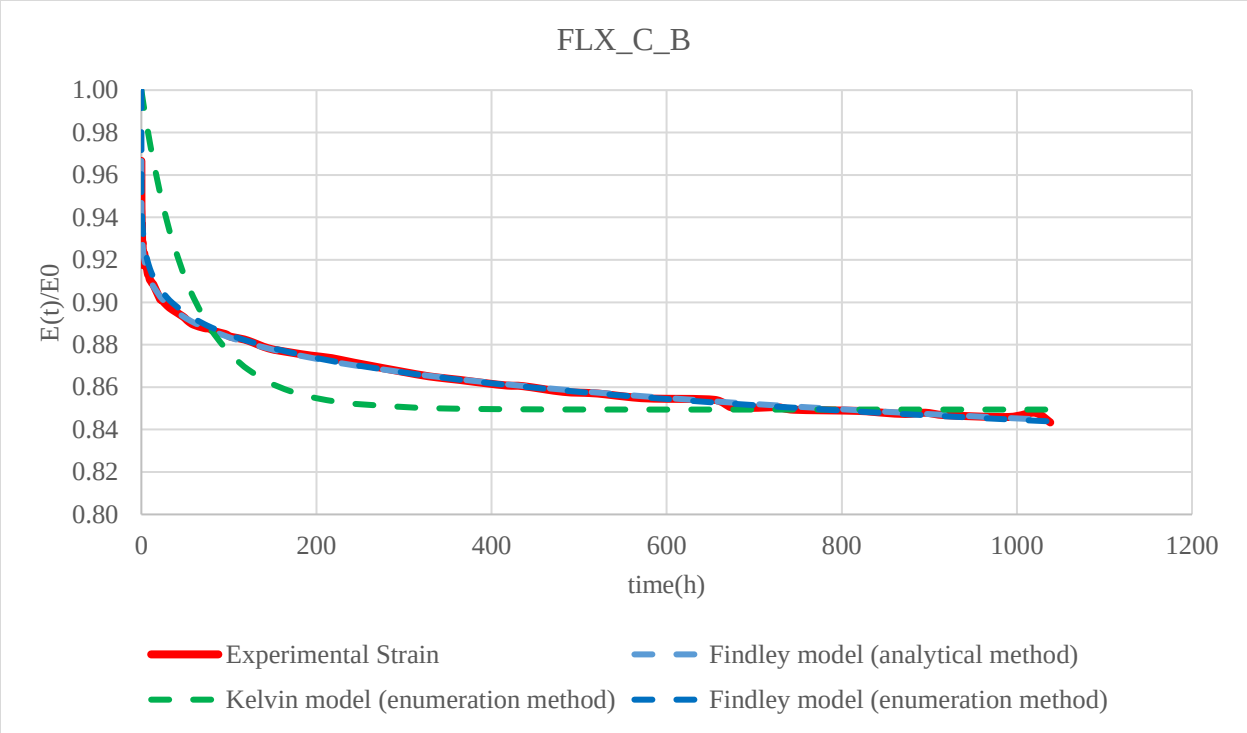

Figure 3.15 Comparison of theoretical and predicted modulus reduction of FLX_C_B

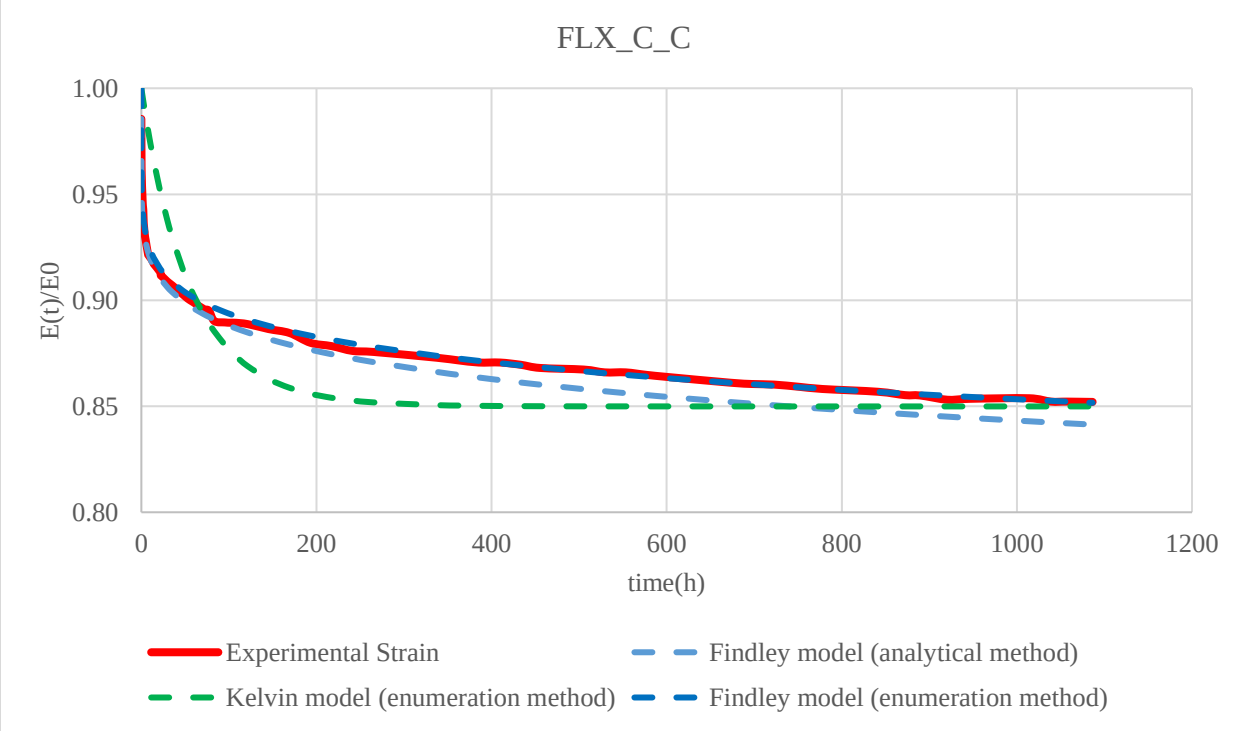

Figure 3.16 Comparison of theoretical and predicted modulus reduction of FLX_C_C

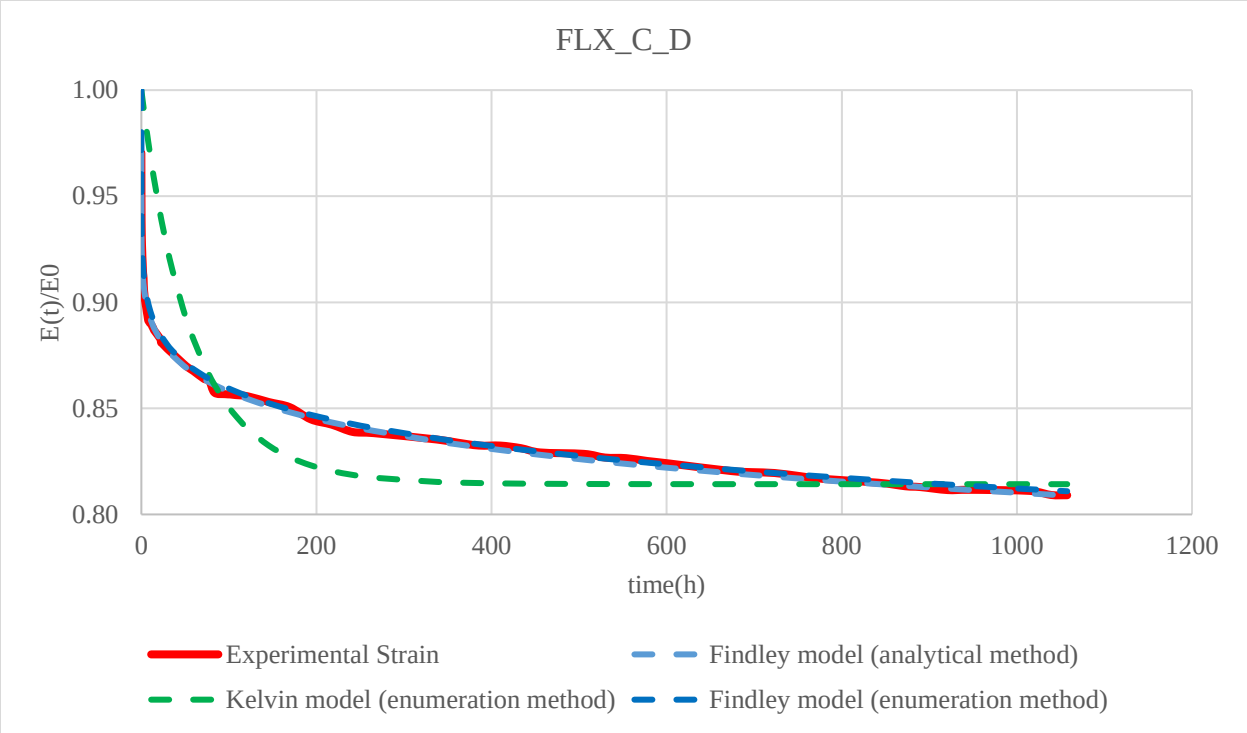

Figure 3.17 Comparison of theoretical and predicted modulus reduction of FLX_C_D

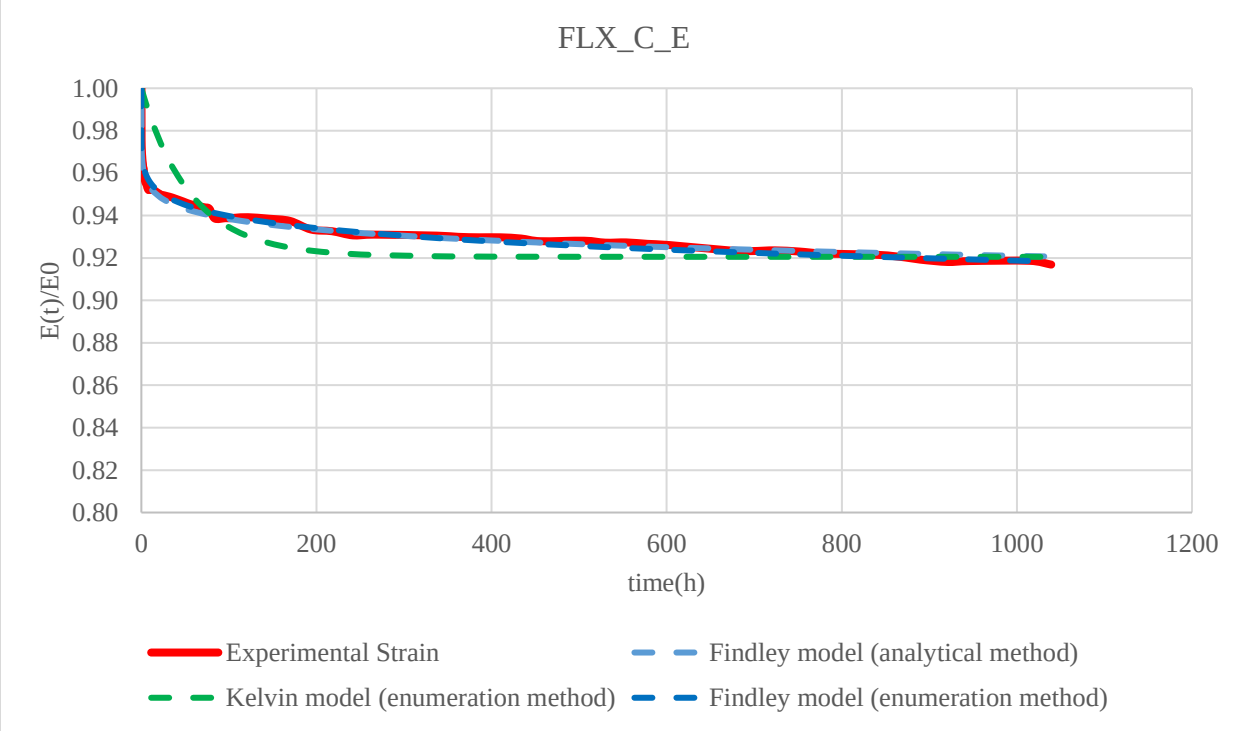

Figure 3.18 Comparison of theoretical and predicted modulus reduction of FLX_C_E

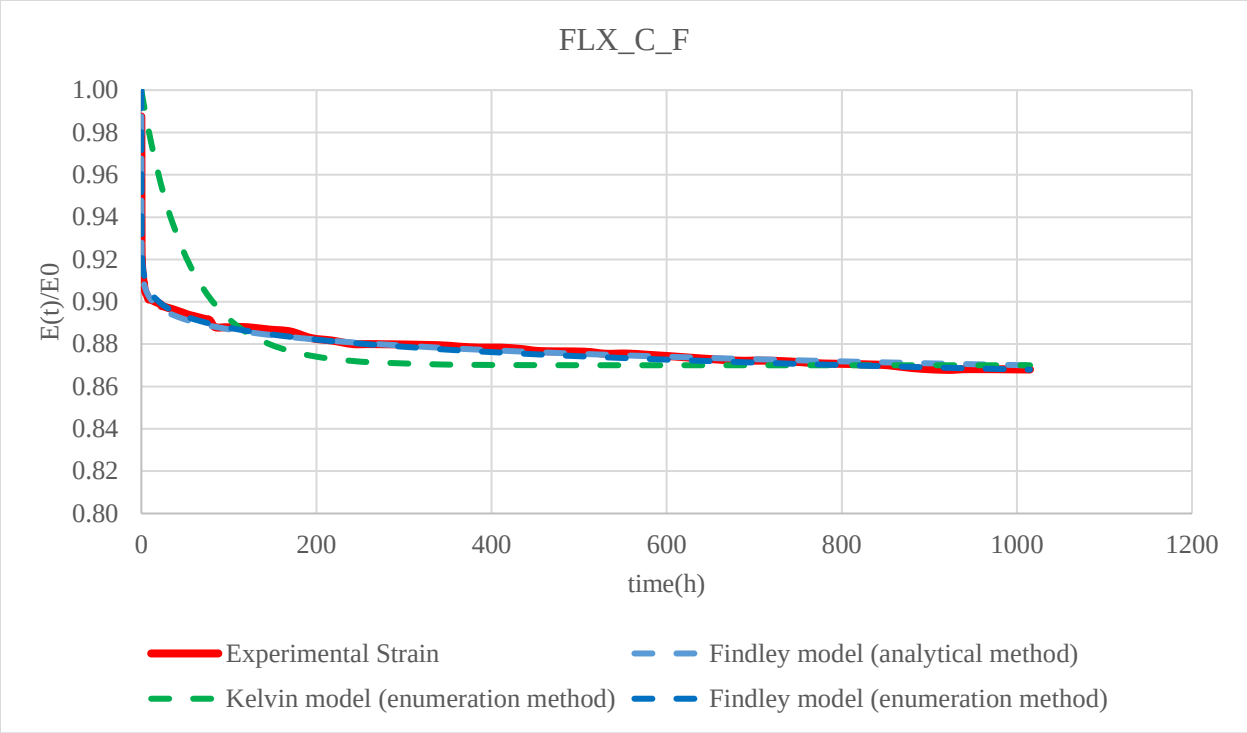

Figure 3.19 Comparison of theoretical and predicted modulus reduction of FLX_C_F

3.4 SUMMARY

In this chapter, flexural creep tests were presented and the results analyzed for theoretical modulus determination. Each model has two moduli to be determined. For the Kelvin standard solid model, an enumeration method written as a MATLAB program was utilized. And for the Findley power law, both an enumeration and analytical method was conducted; the enumeration method showed better predictive capacity. Considering the restriction of application of the Findley power law, the modulus determination process eliminated specimens E/F, which were under higher creep loads. With the average values shown in Table 3.10, further investigation and prediction can be made on aspect of creep buckling.

Table 3.10 Modulus summary from flexural creep tests

	Kelvin standard solid model		Findley power law	
	E_∞ (GPa)	τ (hours)	E_t (GPa)	n
FLX_C_A	18.4	54	340	0.13
FLX_C_B	18.3	63	330	0.15
FLX_C_C	17.9	63	370	0.16
FLX_C_D	16.7	68	250	0.15
FLX_C_E	19.5	60	-	-
FLX_C_F	17.5	60	-	-
Average	18.05	61	322.5	0.15
COV	0.048	0.069	0.138	0.074

4.0 AXIAL BUCKLING

In this chapter, an experimental investigation of creep buckling of slender pGFRP columns is presented and compared to theoretical predictions. The critical short-term buckling load was determined using the graphical method of Southwell (1932). In the long-term experiment, 92% of the critical load was applied to the columns. Time-dependent lateral deflection was recorded and the critical time to creep buckling was obtained. For the theoretical predictions, both the Kelvin standard solid model and Findley power law were utilized, in which the moduli had been determined from the flexural creep tests as summarized in Table 3.10.

4.1 BUCKLING TEST SET-UP

All test specimens were the same GFRP material as described in Section 3.1. Nominal buckling specimen dimensions were 458 x 38.1 x 6.35 mm. Specimens are tested in a pin-ended condition, resulting in a weak axis slenderness ratio, KL/r = 250. Due to the unidirectional roller support conditions, the strong axis slenderness ratio would approach KL/r = 21. The high weak axis slenderness ratio ensures that the specimens will be dominated by global (Euler) buckling behavior and the significantly less slender strong axis should mitigate any bi-axial effects.

Constant axial loading was applied using a lever arm system as shown in Figure 4.1a. As shown in Figure 4.1, the specimen was located 203.2 mm from the lever arm pivot, which was one quarter

of the steel lever arm length; thereby affecting a 4:1 mechanical advantage for the applied dead weights. The steel lever arm was welded from two angles weighing a total of 8.2 kg and its center of gravity was determined to be 415 mm from the pivot. Thus the relationship between the applied load, *w* and load on the column, *P* is (in units of N).

$$P = \frac{415 \text{ x } (8.2 \text{ x } 9.81) + 812.8 \text{ x } 9.81 \text{ x } (\text{w} + P_i)}{203.2} + (9.81)P_f$$
$$= 164.3 + 39.24\ x\ (\text{w} + P_i) + (9.81\ x\ P_f) \quad (4.1)$$

in which P_f = 0.054 kg is the weight of top roller support and P_i = 0.387 kg is the load of free weight hanger.

An overall view of the test setup is shown in Figure 4.1b. The pinned-pinned end support conditions was realised by utilizing steel roller and fixture as shown in Figure 4.1c. A dial gauge was used to measure mid-height lateral deflection. Load was applied using free weights (*w* in Eq. 4.1). Multiple setups were used. Supports beneath the lever arms (Figure 4.1a) were provided to limit the vertical "drop" and therefore prevent the failure of one specimen from impacting an adjacent test. The concrete blocks seen Figure 4.1b were utilized to keep the steel lever arm square so that it did not bind on the pivot or impart a lateral load to the specimen. These were not in contact with the lever arm and thus did not affect loading.

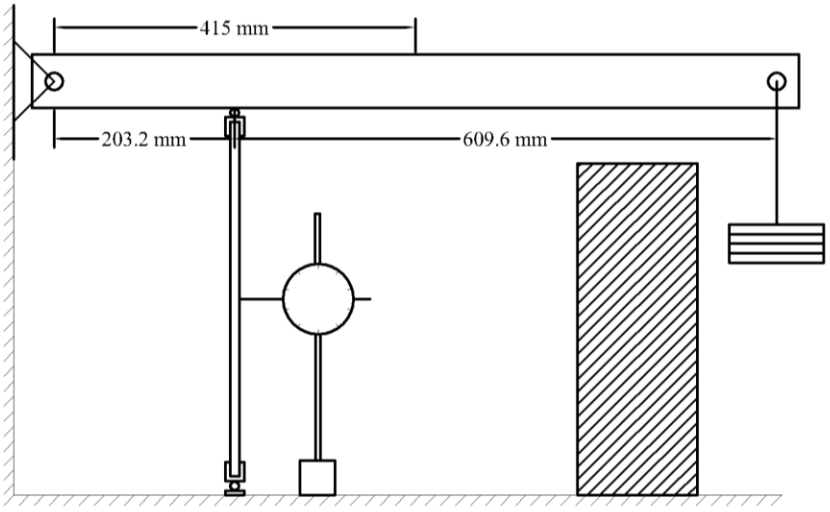

a) schematic view

b) photograph

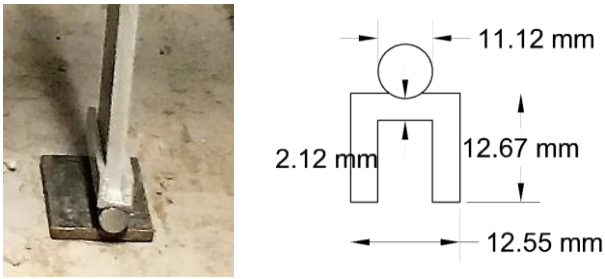

c) roller supports

Figure 4.1 Test Configuration

4.2 SHORT-TERM BUCKLING EXPERIMENTAL PROGRAM

Initially, six specimens were tested to determine their critical buckling load. Results are shown in Table 4.1. All specimens were measured using a digital caliper; measured and nominal dimensions are given in Table 4.1. Due the high weak axis slenderness, greater than *KL/r* = 50, the specimens were expected to demonstrate only global (Euler) buckling behavior about the weak axis (Hashem and Yuan 2001). Therefore, the theoretical critical buckling load may calculated using Euler's formula:

$$P_E = \frac{\pi^2 EI}{(KL)^2} \tag{4.2}$$

in which E is elastic modulus (determined in Section 3.1), I is the weak axis moment of inertia, $K = 1$ is the column effective length factor and L is length of the column. The Euler load, P_E, is the failure load for "perfect" (prismatic, initially straight, concentric load, and ideal (frictionless pins) support conditions) slender columns, for which no lateral deflection occurs before buckling.

The experimentally-determined critical load was determined using a Southwell plot (Southwell 1932), which is a widely-used graphical method (Hewson,1978; Barbero and Tomblin, 1992; Scott and Zureick, 1997; Bennett, 2005) to obtain the critical load of a slender column without having to achieve (or specifically define) column failure. This method accounts for initial imperfection and load eccentricity. When the applied load, P, approaches the critical load, P_{cr}, it was observed by Southwell that

$$\delta = \frac{c}{\frac{P_{cr}}{P} - 1} = P_{cr}\frac{\delta}{P} - c \tag{4.3}$$

in which δ is the measured mid-height lateral deflection and c is a constant. According to Equation 4.3, if δ is plotted against δ /P the resulting slope is the critical load, P_{cr}, of the column accounting

for all imperfections. *c* is a measure of the effect of all imperfections. In the short-term buckling tests, lateral deflection was recorded with load until load was close to the calculated Euler load. Figure 4.2 presents an example of the Southwell plot of specimen CB2. Because of the high slenderness, buckling is elastic; three repetitions were conducted for each specimen. Excellent repeatability and linearity was evident in all tests and can be seen for specimen CB2 in Figure 4.2. Additionally, the tests were controlled so that lateral displacements were limited to less than L/400; thereby limiting damage to the specimens allowing them to be subsequently tested for creep buckling as described in the next section. This is a significant advantage of using the Southwell method – specimens may be reused, thus actual buckling loads are known.

Both predicted Euler load and experimental critical load are given in Table 4.1. As can be seen, the experimental buckling loads are marginally greater than the Euler loads. In these experiments, the specimens had no measurable imperfections and great care was taken to ensure concentric loading. The greater experimental loads are primarily attributed to the restraint provided by friction at the pinned connections; thus the actual value of the effective length factor, *K* is likely better give and 0.99 to 0.98. Since this is a comparative study, this distinction is not critical.

Table 4.1 Short-term critical buckling load

	L (mm)	b (mm)	d (mm)	slenderness ratio	P_E (N)	P_{exp} (N)	$\frac{P_{exp}}{P_E}$ %
Nominal	457.20	38.10	6.35	249	802	-	-
CB1	452.12	38.84	6.44	243	871	865	99
CB2	457.20	37.88	6.17	257	733	740	101
CB3	452.12	38.86	6.19	253	774	803	104
CB4	452.12	38.94	6.25	250	801	822	103
CB5	457.20	37.93	6.08	260	702	792	113
CB6	457.20	37.93	6.10	259	709	734	104

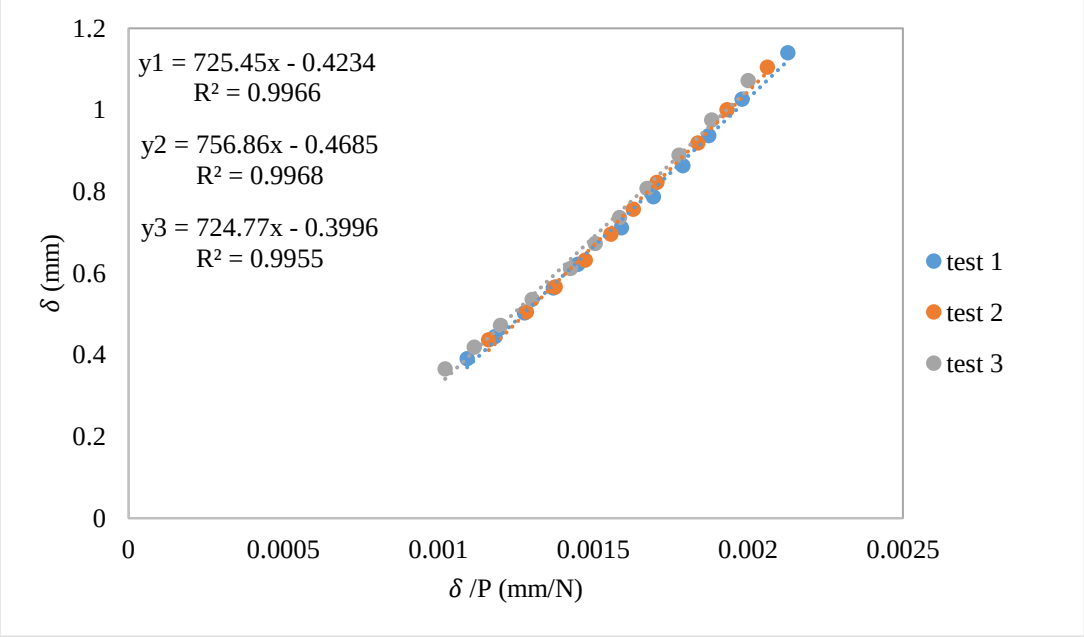

Figure 4.2 Southwell plot of specimen CB2

4.3 LONG-TERM BUCKLING EXPERIMENTAL PROGRAM

For all six specimens described in Section 4.2, following determination of their critical buckling loads using the Southwell method, 92% of the critical load was applied and lateral deflections were recorded at the following intervals:

- Immediately after loading;
- 5 min increments for the first three hours;
- 30 min increments subsequently.

Dial gage readings were logged digitally using timed photographs. The critical buckling time was determined as that when the specimen physically exhibited a large increase in lateral displacement and an inability to continue to resist the applied load (loss of equilibrium). In each case, buckling was clearly evident as is shown below. During the creep tests, the ambient environmental conditions were constant as required by ASTM D2990-09. The temperature remained at 21 ± 1^{o}C and relative humidity was 53 ± 5%.

Table 4.2 presents the applied loads and critical buckling time of the columns. Specimens CB1 and CB3 buckled during loading, which likely resulted from a combination of specimen initial imperfection and some non-concentric load application while the system was being loaded. For the other four columns, the buckling time varies from 6.5 to 213.4 hours.

Table 4.2 Critical buckling time in the test

	P_{exp}	P	P/P_{exp}	Critical Buckling Time (h)
CB1	865	796	92	-
CB2	740	678	92	46.0
CB3	803	741	92	-
CB4	822	759	92	6.5
CB5	792	732	92	213.4
CB6	734	678	92	182.8

Lateral deflection curves for specimen CB2, CB4, CB5 and CB6 are presented in Figures 4.3-4.6, respectively. The time-dependent lateral deflection exhibits the classic creep deformation behavior illustrated in Figure 2.1. Deformation increases quickly immediately following loading (primary

creep deformation). The deformation rate is reduced and relatively constant during the secondary deformation phase and increases rapidly (tertiary deformation) as the specimen approaches failure.

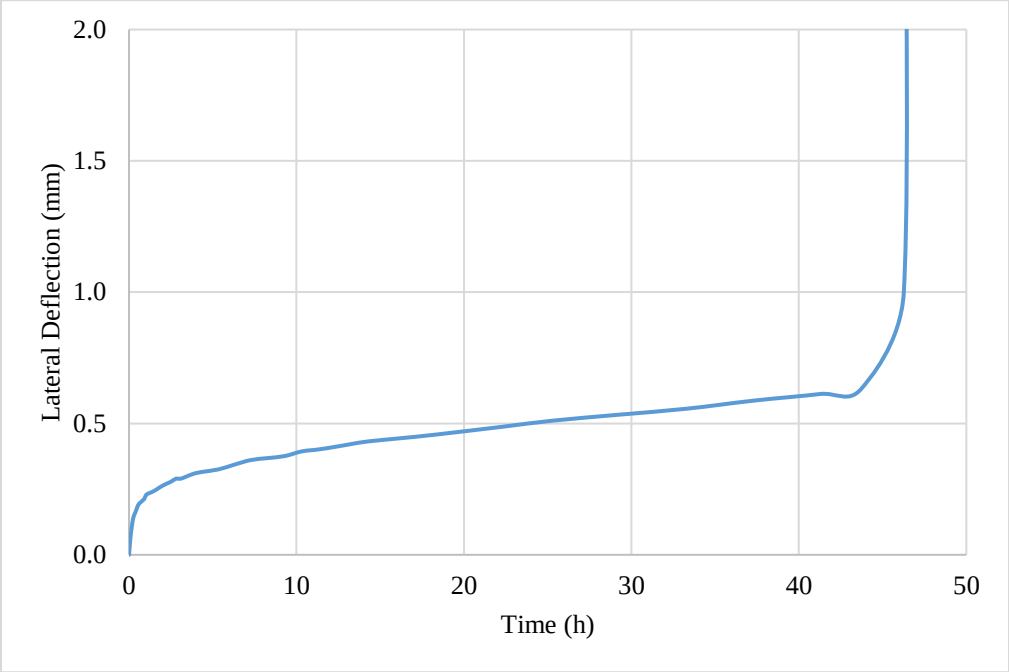

Figure 4.3 Lateral Deflection of Specimen CB2

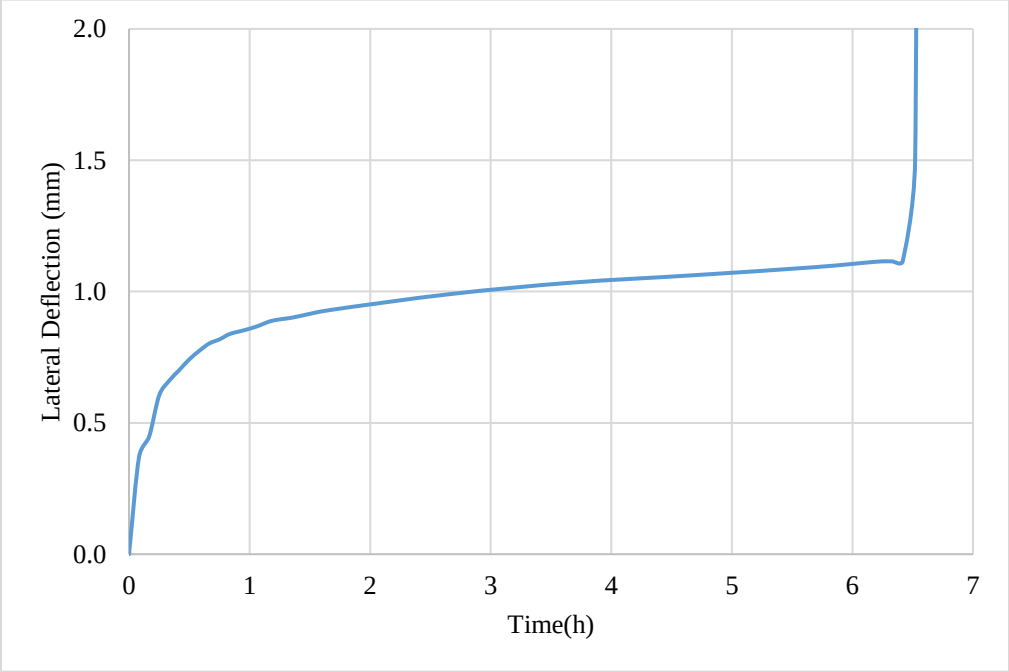

Figure 4.4 Lateral Deflection of Specimen CB4

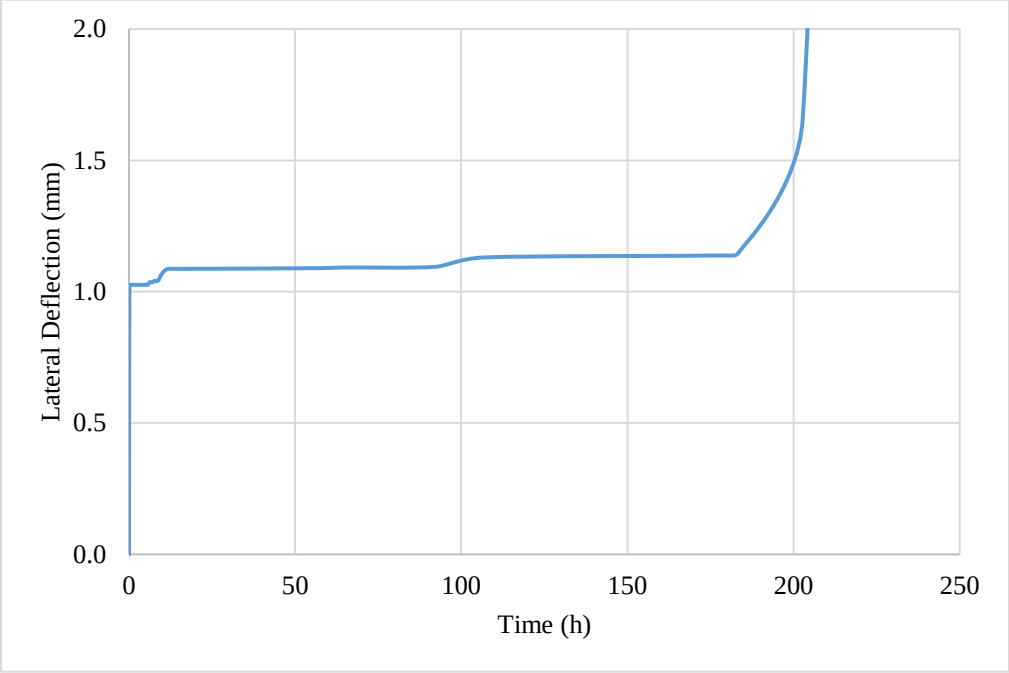

Figure 4.5 Lateral Deflection of Specimen CB5

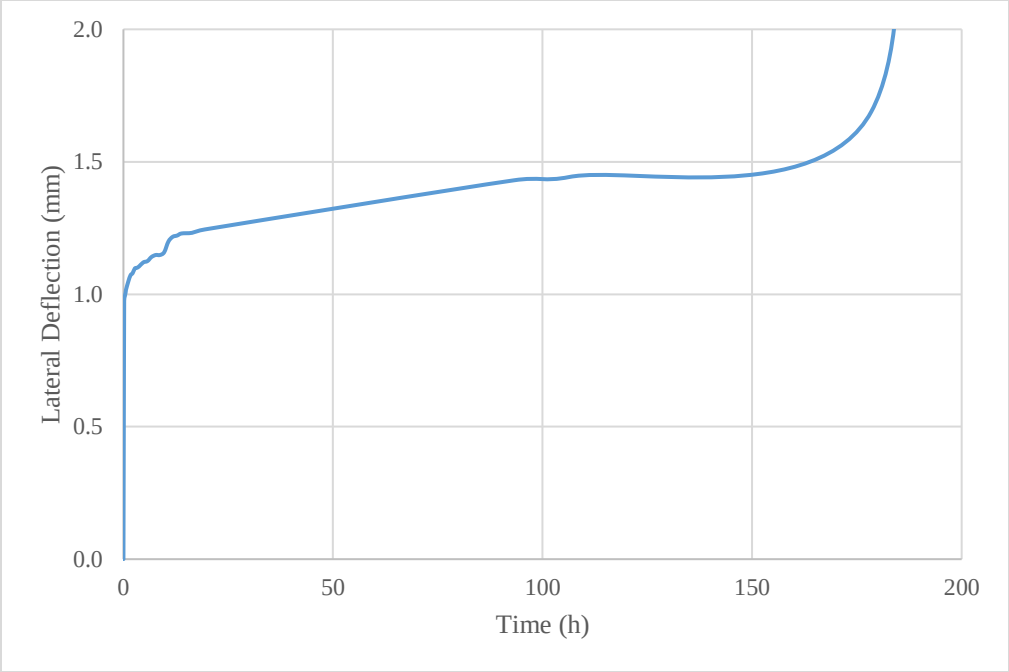

Figure 4.6 Lateral Deflection of Specimen CB6

4.4 ANALYSIS AND DISCUSSION

In Section 2.4, an equation for theoretical prediction of time-dependent lateral deflection ratio of pGFRP columns was presented (Equation 2.32) that was derived based on Kelvin standard solid model in viscoelastic theory. Due to the good fitting effect of Findley power law in flexural creep tests reported in Chapter 3, this empirical model was utilized to derive another equation of deflection ratio $f^F(t)$ in this section.

In the Kelvin standard solid model, the long-term stress-strain relationship can be expressed in differential form with a differential operator. However, it is hard to analytically represent the differential expression for Findley power law. Since the long-term strain-stress relation has been

presented in Equation 2.12, replacing E with $E(t)$ in Equation 2.25, the governing equation in both space and time could be derived as

$$v'' - v_0'' + \tau_r \dot{v}'' + \frac{P}{E_0 I} v + \frac{P t^n}{E_t I} v = 0 \tag{4.4}$$

Assuming the form of v given in Equation 2.29, function $f^F(t)$ is obtained as

$$f^F(t) = \frac{1}{1 - P/P_{E_0} - P t^n / P_{E_t}} = \frac{1}{1 - \mathrm{P}/P_{E(t)}} \tag{4.5}$$

in which

$P_{E_t} = \pi^2 E_t I / L^2$ and

$P_{E(t)} = \pi^2 E(t) I / L^2$.

In Equation 4.5, the boundary conditions of $f^F(t)$ are both satisfied. For $t = 0$, $f^F(0) = \frac{1}{1 - P/P_{E_0}} = f^K(0)$ and for $t \to \infty$, $f^F(\infty) = \frac{1}{1 - P/P_{E_\infty}} = f^K(\infty)$. With Equation 2.32, Equation 4.5 and model parameters presented in Table 3.10, prediction based on Kelvin standard solid model and Findley power law for the lateral deflection ratio time history as well as critical time of creep buckling can be conducted. Figure 4.10 and Figure 4.11 are the theoretically predicted deflection ratio time histories calculated for the pGFRP tested here having nominal dimensions. As shown in Figure 4.7, the *f(t)* curve representing Kelvin model did not indicate obvious buckling (rapid transition from secondary to tertiary creep behavior (Figure 2.1)) but rather a gradual increase in *f(t)*. This is due to the exponential form of Equation 2.32. In contrast, the *f(t)* curve representing the Findley model, shown in Figure 4.8, exhibits a sudden increase of deflection ratio *f(t)* and a fairly obvious critical time. Considering that it is hard to define buckling with the value *f(t)*, the buckling time from the curve of Kelvin model was determined at which $f^K(t) = f^F(t=6.5)$. $f^F(t=6.5)$ is approximately the initiation of buckling seen in the Findley curve (Figure 4.8) corresponding to

the transition from secondary to tertiary creep. The critical buckling time of the specimens was predicted to be about 269 and 6.5 hours, for the Kelvin and Findley predictions, respectively. The experimentally observed values varied from 6.5 to 214 hours (Table 4.2); thus the models appear top bound the observed behavior quite well with the Findley model falling on the conservative side.

The reason for the large difference between predicted results of these two models could be explained by the predicted longitudinal modulus reduction in flexural creep tests (Figure 3.9). For all the six specimens, the longitudinal modulus E(t) predicted by the Findley model kept reducing while E(t) predicted by the Kelvin model approaches a constant value E_∞. By comparison of the functions predicted by the two models (Equation 2.32 and Equation 4.5, respectively), the power term was the denominator in Findley model. When $P_{E(t)}$ approached P in the Findley model, the function *f(t)* would increase extremely. However in the Kelvin model, the exponential term was the numerator, since τ_b was negative when $P > P_{E_\infty}$. Thus $f^K(t)$ grew slowly and predicted much longer critical time.

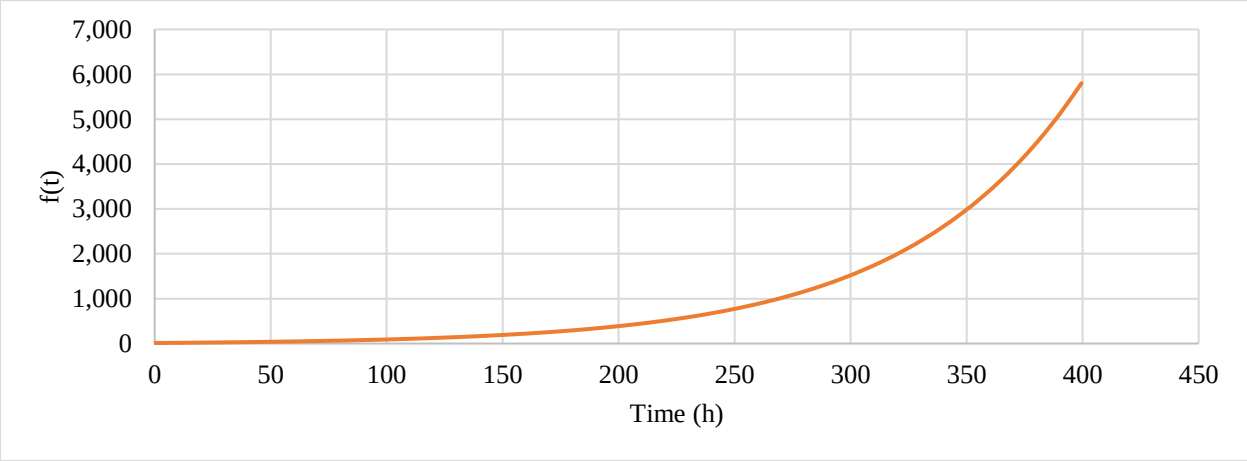

Figure 4.7 Predicted curve of *f(t)* for nominal specimen with Kelvin Model

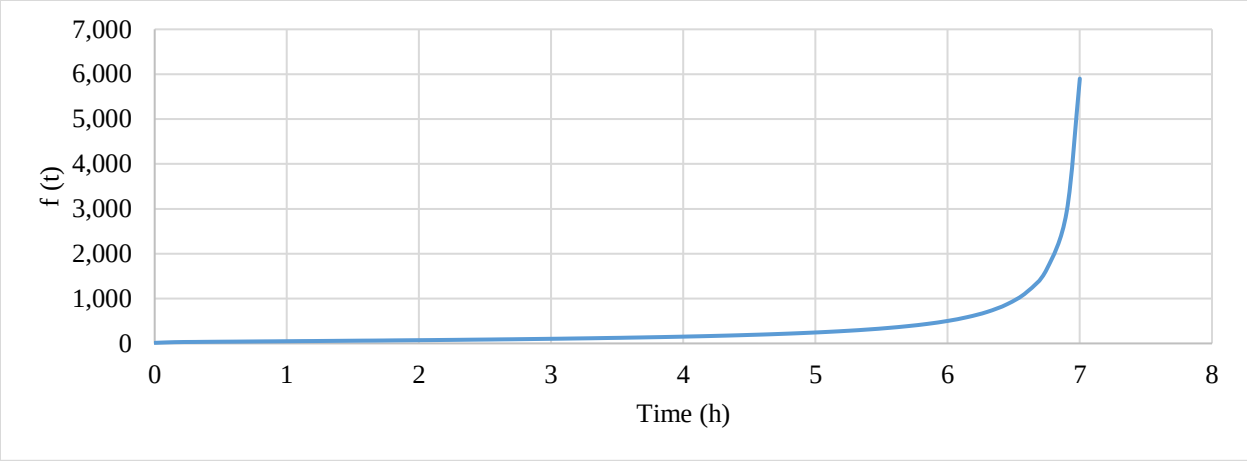

Figure 4.8 Predicted curve of *f(t)* for nominal specimen with Findley power law

4.5 SUMMARY

In this chapter, experimental investigation as well as theoretical prediction of six slender column specimens' creep buckling behaviors was presented. In the experimental parts, short-term critical load for the six specimens were determined using Southwell's method. Following this, creep buckling tests at 92% of experimental short-term critical load were conducted. During the test, lateral deflection readings were taken regularly and critical time of buckling was recorded. As for theoretical predictions, both the Kelvin standard solid model and Findley power law were utilized to derive the deflection ratio function $f(t)$. The expression derived based on the Findley power law was proposed in this work. The Findley model provided a more conservative prediction of critical time.

5.0 CONCLUSION AND FUTURE STUDY

5.1 CONCLUSION

Based on experimental and theoretical results in this work, the following conclusions can be made:

1) In both flexural and axial creep tests, the creep behaviors were consistent with the classic creep deformation behavior (Figure 2.1). While the creep buckling test results showed all three stages of creep, the flexural creep tests only exhibited the primary and secondary stages because the stress levels were not high enough to cause failure in the relatively short 1000 hour tests.
2) In the flexural creep tests, strain and deflection readings kept increasing in the 1000-hour test. And the increment of strain and deflection was larger as the stress level got higher. At the same time, longitudinal modulus reduced with time and approached 84% of the initial value following 1000 hours of loading.
3) For 1000-hour flexural creep tests, the Findley power law provided very good descriptive results while the Kelvin standard solid model did not fit well with experimental results. For the Findley power law, enumeration method resulted in better predictive results than the analytical method.

4) Based on the summary data presented in table 3.10, it is felt that the 1000-hour test was adequate to estimate long term modeling parameters of the pGFRP, particularly for the Findley power law. Such a test duration is considered practical.
5) The modified creep buckling equation based on the Findley power law is able to predict the shape of time-dependent mid-height lateral deflection as well as critical buckling time of slender pGFRP columns under concentric load.
6) According to moduli determined using the Findley model enumeration method, application of the Findley model should be limited to lower permanent (creep) loads. In this study, the model worked well for P/P_{ult} = 0.25 but was inadequate for P/P_{ult} = 0.38. Further study is required to refine the limit of application of this model.
7) For axial creep tests, critical time prediction made from the Kelvin and Findley models differed significantly. This difference could be explained by the different equation form of the two models. When load level was 92% of critical load, neither model offered consistent critical time prediction since the experimental results varied. But generally, the critical time predicted by the Findley power law was more conservative.

5.2 RECOMMENDATION FOR FUTURE STUDY

On the basis of investigation in this work, the following recommendations for future study are made:

1) As mentioned in Section 2.4, the shape of function $f(t)$ predicted by the Kelvin model was different for $P < P_{E_\infty}$ and $P > P_{E_\infty}$. In this work, only one load level (92%) in condition $P > P_{E_\infty}$ was investigated since the research object was to illustrate the critical buckling

time. For more comprehensive investigation of the creep buckling behaviors of pGFRP columns as well as descriptive models' validity, more load levels should be considered.

2) This work focused on the prediction of critical time in creep buckling. At the same time, the lateral deflection increase over time is another important issue since typically the applied load in practice will be a significantly smaller proportion of critical load than was tested here. Based on the expression of function $f(t)$, the function of lateral deflection $v(t)$ could be derived according to Equation 2.29.

APPENDIX A

MATLAB PROGRAM FOR MODULI DETERMINATION

A.1 KELVIN MODEL ENUMERATION PROGRAM

```
%Kelvin Model Prediction

clear all

L=304.8;
a=116.84;
g=9.81;
load1=50;
load2=100;
load3=150;

%A
E0_A=21100;
b_A=38.74;
t_A=6.19;
I_A=b_A*t_A^3/12;%mm^4
Pmid_A=load2/2/2.2*g;%N
Mmid_A=Pmid_A*a;
stressmid_A=Mmid_A*(t_A/2)/I_A;

%Adata
hours_A=xlsread('flexural results.xlsx',4,'F5:F84');
strain_AT=xlsread('flexural results.xlsx',4,'G5:G84');
strain_AC=xlsread('flexural results.xlsx',4,'H5:H84');
stress_AC=xlsread('flexural results.xlsx',4,'I5:I84');
stress_AT=xlsread('flexural results.xlsx',4,'J5:J84');
```

```
%B
E0_B=20500;
b_B=38.8;
t_B=6.2;
I_B=b_B*t_B^3/12;%mm^4
Pmid_B=load2/2/2.2*g;%N
Mmid_B=Pmid_B*a;
stressmid_B=Mmid_B*(t_B/2)/I_B;
%Bdata
hours_B=xlsread('flexural results.xlsx',4,'N5:N85');
strain_BT=xlsread('flexural results.xlsx',4,'O5:O85');
strain_BC=xlsread('flexural results.xlsx',4,'P5:P85');
stress_BC=xlsread('flexural results.xlsx',4,'Q5:Q85');
stress_BT=xlsread('flexural results.xlsx',4,'R5:R85');

%C
E0_C=21200;
b_C=38.7;
t_C=6.2;
I_C=b_C*t_C^3/12;%mm^4
Pmid_C=load3/2/2.2*g;%N
Mmid_C=Pmid_C*a;
stressmid_C=Mmid_C*(t_C/2)/I_C;
%Cdata
hours_C=xlsread('flexural results.xlsx',4,'V5:V86');
strain_CT=xlsread('flexural results.xlsx',4,'W5:W86');
strain_CC=xlsread('flexural results.xlsx',4,'X5:X86');
stress_CC=xlsread('flexural results.xlsx',4,'Y5:Y86');
stress_CT=xlsread('flexural results.xlsx',4,'Z5:Z86');

%D
E0_D=20100;
b_D=38.8;
t_D=6.2;
I_D=b_D*t_D^3/12;%mm^4
Pmid_D=load3/2/2.2*g;%N
Mmid_D=Pmid_D*a;
stressmid_D=Mmid_D*(t_D/2)/I_D;
%Ddata
hours_D=xlsread('flexural results.xlsx',4,'AD5:AD87');
strain_DT=xlsread('flexural results.xlsx',4,'AE5:AE87');
strain_DC=xlsread('flexural results.xlsx',4,'AF5:AF87');
stress_DC=xlsread('flexural results.xlsx',4,'AG5:AG87');
stress_DT=xlsread('flexural results.xlsx',4,'AH5:AH87');

%E
E0_E=21100;
```

```
b_E=39.0;
t_E=6.3;
I_E=b_E*t_E^3/12;%mm^4
Pmid_E=load1/2/2.2*g;%N
Mmid_E=Pmid_E*a;
stressmid_E=Mmid_E*(t_E/2)/I_E;
%Edata
hours_E=xlsread('flexural results.xlsx',4,'AL5:AL83');
strain_ET=xlsread('flexural results.xlsx',4,'AM5:AM83');
strain_EC=xlsread('flexural results.xlsx',4,'AN5:AN83');
stress_EC=xlsread('flexural results.xlsx',4,'AO5:AO83');
stress_ET=xlsread('flexural results.xlsx',4,'AP5:AP83');

%F
E0_F=21500;
b_F=39.0;
t_F=6.2;
I_F=b_F*t_F^3/12;%mm^4
Pmid_F=load1/2/2.2*g;%N
Mmid_F=Pmid_F*a;
stressmid_F=Mmid_F*(t_F/2)/I_F;
%Fdata
hours_F=xlsread('flexural results.xlsx',4,'AT5:AT83');
strain_FT=xlsread('flexural results.xlsx',4,'AU5:AU83');
strain_FC=xlsread('flexural results.xlsx',4,'AV5:AV83');
stress_FC=xlsread('flexural results.xlsx',4,'AW5:AW83');
stress_FT=xlsread('flexural results.xlsx',4,'AX5:AX83');


hours=hours_A;
strain=strain_AC;
stress=stress_AC;
E0=E0_A;
[No_of_data,column]=size(hours);

ini_Einf=15000;
int_Einf=100;
final_Einf=20000;

for Einf=ini_Einf:int_Einf:final_Einf
    for tau=1:500
        for i=1:No_of_data
            strain_K(i,1)=(1/Einf-(1/Einf-1/E0)*exp(-
hours(i,1)/tau))*stress(i,1)*10^6;
        end
```

```
        for i=1:No_of_data
            if i<40
                sq(i)=(strain_K(i,1)-strain(i,1))^2;
            else if i<70
                sq(i)=(strain_K(i,1)-strain(i,1))^2*1600;
                else
                    sq(i)=(strain_K(i,1)-strain(i,1))^2*16000;
                end
            end
        end

        sqsum_K((Einf-ini_Einf)/int_Einf+1,tau)=sum(sq);
    end
    lsqmin_K=min((sqsum_K),[],2);
end
lsqmin_K=min((lsqmin_K),[],1);
sqsum_K=fix(sqsum_K.*1000);
lsqmin_K=fix(lsqmin_K*1000);
[Row,Col]=find(sqsum_K==lsqmin_K);
Einf=(Row-1)*int_Einf+ini_Einf
tau=Col
```

A.2 FINDLEY MODEL ENUMERATION PROGRAM

```
%Findley Model Prediction
clear all


L=304.8;
a=116.84;
g=9.81;
load1=50;
load2=100;
load3=150;

%A
E0_A=21061;
b_A=38.74;
t_A=6.19;
I_A=b_A*t_A^3/12;%mm^4
Pmid_A=load2/2/2.2*g;%N
Mmid_A*a;
```

```
stressmid_A=Mmid_A*(t_A/2)/I_A;

%Adata
hours_A=xlsread('flexural results.xlsx',4,'F5:F84');
strain_AT=xlsread('flexural results.xlsx',4,'G5:G84');
strain_AC=xlsread('flexural results.xlsx',4,'H5:H84');
stress_AC=xlsread('flexural results.xlsx',4,'I5:I84');

%B
E0_B=20500;
b_B=38.8;
t_B=6.2;
I_B=b_B*t_B^3/12;%mm^4
Pmid_B=load2/2/2.2*g;%N
Mmid_B=Pmid_B*a;
stressmid_B=Mmid_B*(t_B/2)/I_B;
%Bdata
hours_B=xlsread('flexural results.xlsx',4,'N5:N85');
strain_BT=xlsread('flexural results.xlsx',4,'O5:O85');
strain_BC=xlsread('flexural results.xlsx',4,'P5:P85');
stress_BC=xlsread('flexural results.xlsx',4,'Q5:Q85');

%C
E0_C=21200;
b_C=38.7;
t_C=6.2;
I_C=b_C*t_C^3/12;%mm^4
Pmid_C=load3/2/2.2*g;%N
Mmid_C=Pmid_C*a;
stressmid_C=Mmid_C*(t_C/2)/I_C;
%Cdata
hours_C=xlsread('flexural results.xlsx',4,'V5:V86');
strain_CT=xlsread('flexural results.xlsx',4,'W5:W86');
strain_CC=xlsread('flexural results.xlsx',4,'X5:X86');
stress_CC=xlsread('flexural results.xlsx',4,'Y5:Y86');

%D
E0_D=20100;
b_D=38.8;
t_D=6.2;
I_D=b_D*t_D^3/12;%mm^4
Pmid_D=load3/2/2.2*g;%N
Mmid_D=Pmid_D*a;
stressmid_D=Mmid_D*(t_D/2)/I_D;
%Ddata
hours_D=xlsread('flexural results.xlsx',4,'AD5:AD87');
strain_DT=xlsread('flexural results.xlsx',4,'AE5:AE87');
```

```
strain_DC=xlsread('flexural results.xlsx',4,'AF5:AF87');
stress_DC=xlsread('flexural results.xlsx',4,'AG5:AG87');

%E
E0_E=21100;
b_E=39.0;
t_E=6.3;
I_E=b_E*t_E^3/12;%mm^4
Pmid_E=load1/2/2.2*g;%N
Mmid_E=Pmid_E*a;
stressmid_E=Mmid_E*(t_E/2)/I_E;
%Edata
hours_E=xlsread('flexural results.xlsx',4,'AL5:AL83');
strain_ET=xlsread('flexural results.xlsx',4,'AM5:AM83');
strain_EC=xlsread('flexural results.xlsx',4,'AN5:AN83');
stress_EC=xlsread('flexural results.xlsx',4,'AO5:AO83');

%F
E0_F=21500;
b_F=39.0;
t_F=6.2;
I_F=b_F*t_F^3/12;%mm^4
Pmid_F=load1/2/2.2*g;%N
Mmid_F=Pmid_F*a;
stressmid_F=Mmid_F*(t_F/2)/I_F;
%Fdata
hours_F=xlsread('flexural results.xlsx',4,'AT5:AT83');
strain_FT=xlsread('flexural results.xlsx',4,'AU5:AU83');
strain_FC=xlsread('flexural results.xlsx',4,'AV5:AV83');
stress_FC=xlsread('flexural results.xlsx',4,'AW5:AW83');



hours=hours_F;
strain=strain_FC;
stress=stress_FC;
E0=E0_F;
[No_of_data,column]=size(hours);

ini_Et=100000;
int_Et=10000;
final_Et=700000;

for Et=ini_Et:int_Et:final_Et
    for n=1:30
        for i=1:No_of_data
```

```
strain_F(i,1)=(1/E0+(hours(i,1)^(n/100))/Et)*stress(i,1)*10^6;
        end


        for i=1:No_of_data
            if i<40
                sq(i)=(strain_F(i,1)-strain(i,1))^2;
            else
                sq(i)=(strain_F(i,1)-strain(i,1))^2*1600;
            end
        end

        sqsum_F(((Et-ini_Et)/int_Et+1),n)=sum(sq);
    end
    lsqmin_F=min((sqsum_F),[],2);
end
lsqmin_F=min((lsqmin_F),[],1);
sqsum_F=fix(sqsum_F.*1000);
lsqmin_F=fix(lsqmin_F*1000);
[Row,Col]=find(sqsum_F==lsqmin_F);
Et=(Row-1)*int_Et+ini_Et
n=Col/100
```

APPENDIX B

FINDLEY POWER LAW LOGARITHM PLOTS

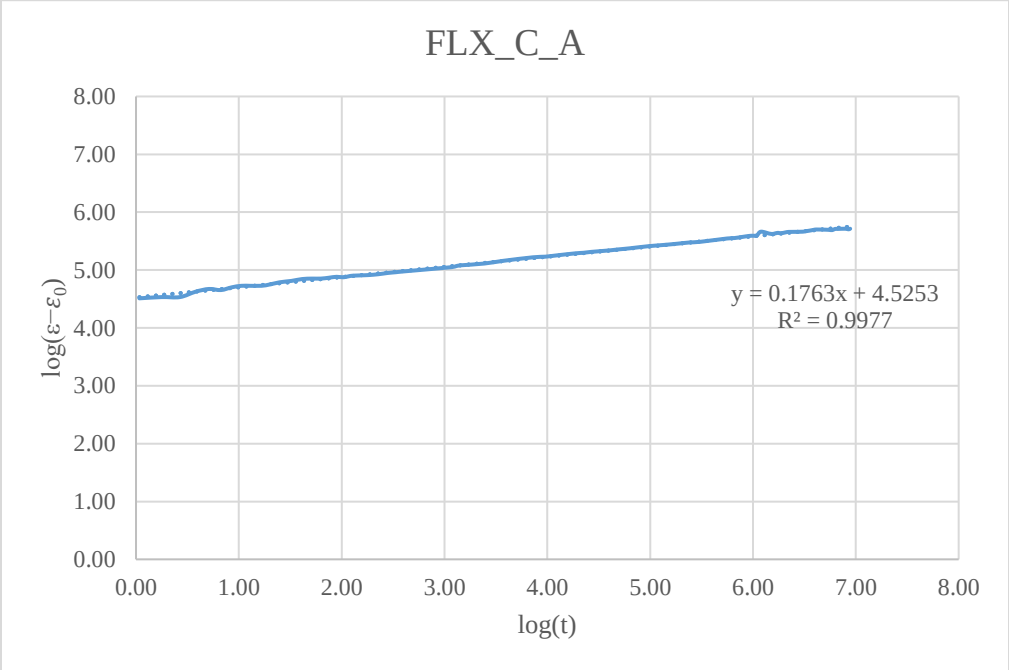

Figure A.1 Plot of log(ε−ε_0) to log(t) of FLX_C_A

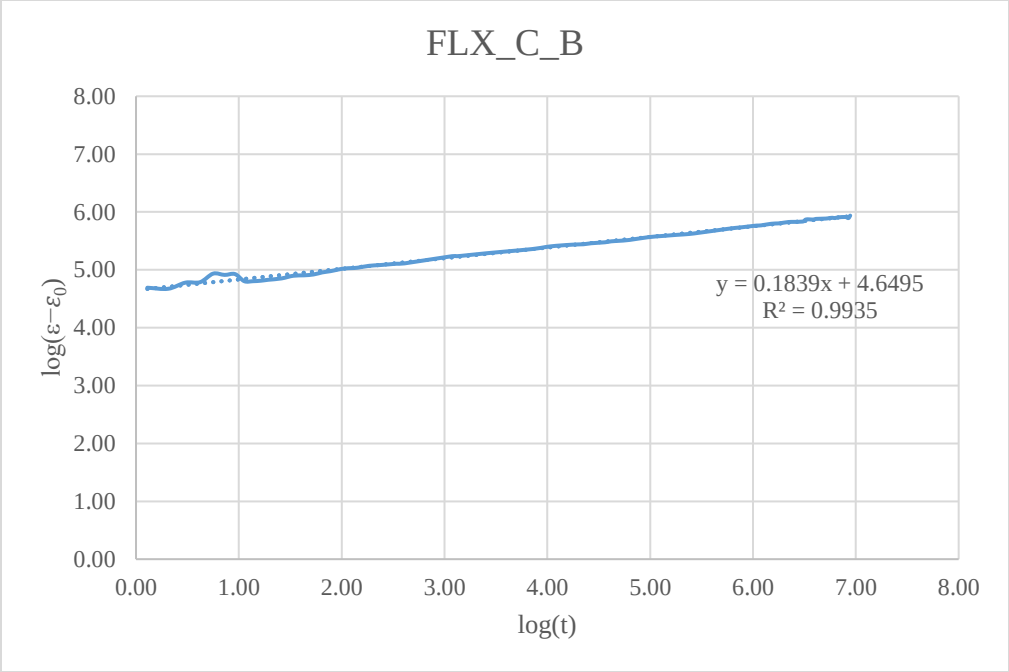

Figure A.2 Plot of log(ε−ε_0) to log(t) of FLX_C_B

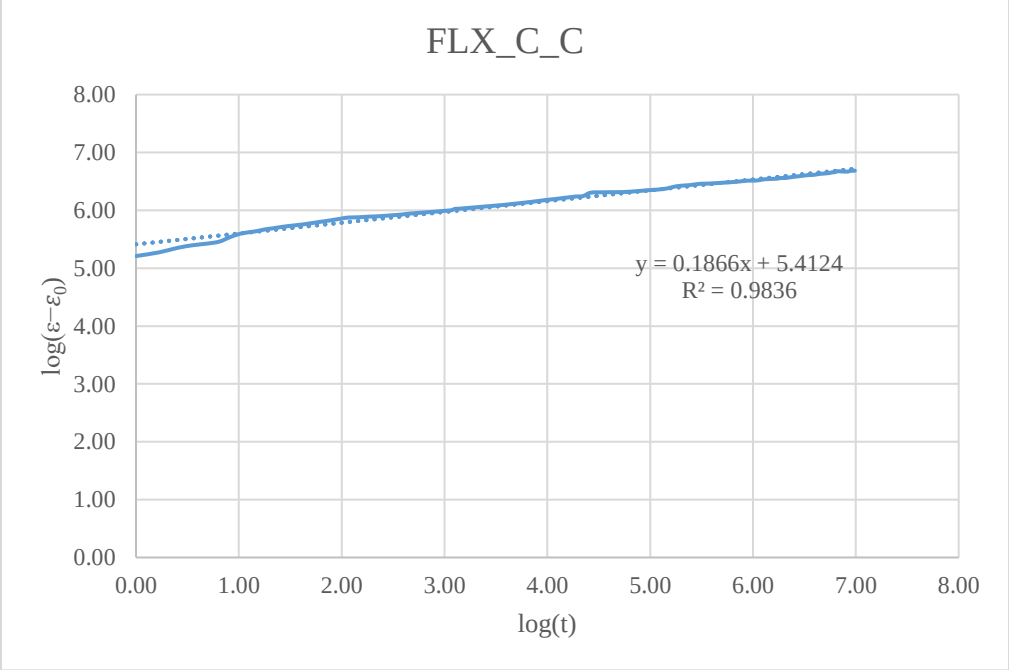

Figure A.3 Plot of log(ε−ε_0) to log(t) of FLX_C_C

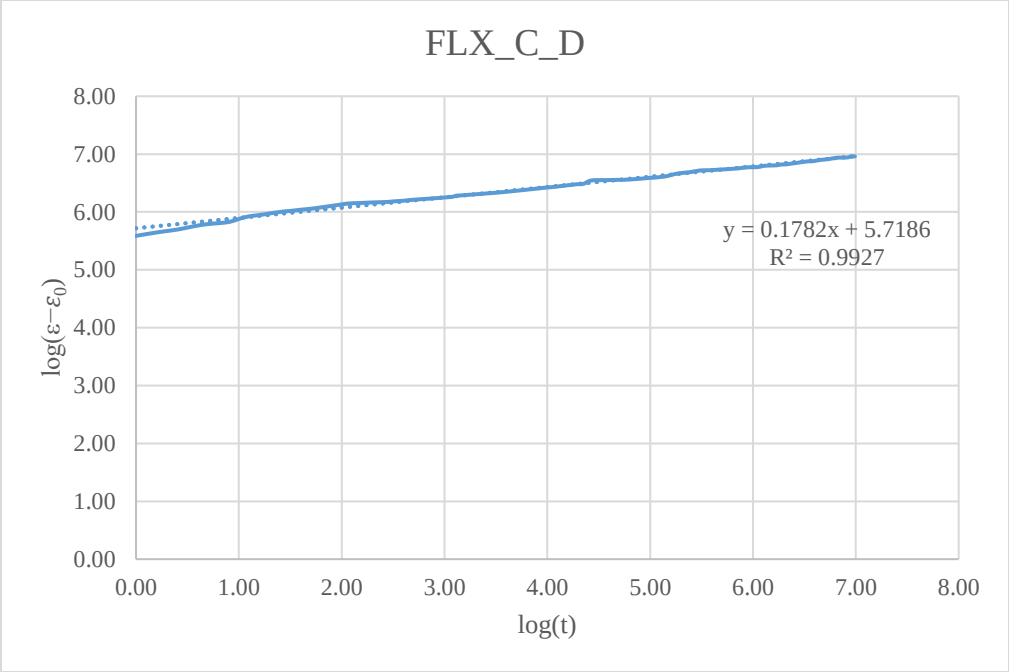

Figure A.4 Plot of log(ε−ε_0) to log(t) of FLX_C_D

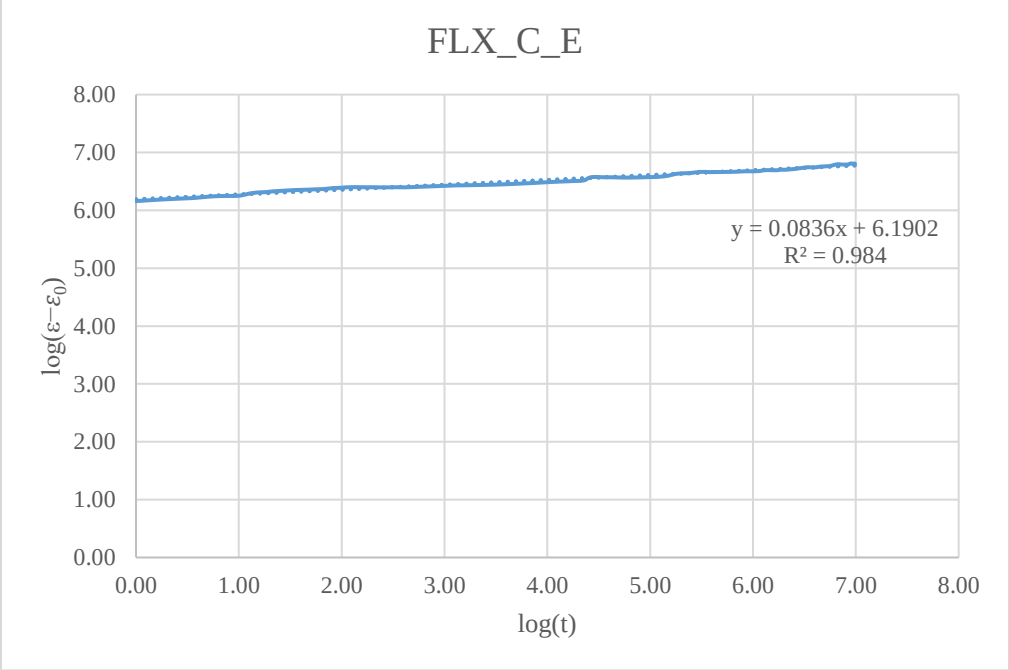

Figure A.5 Plot of log(ε−ε_0) to log(t) of FLX_C_E

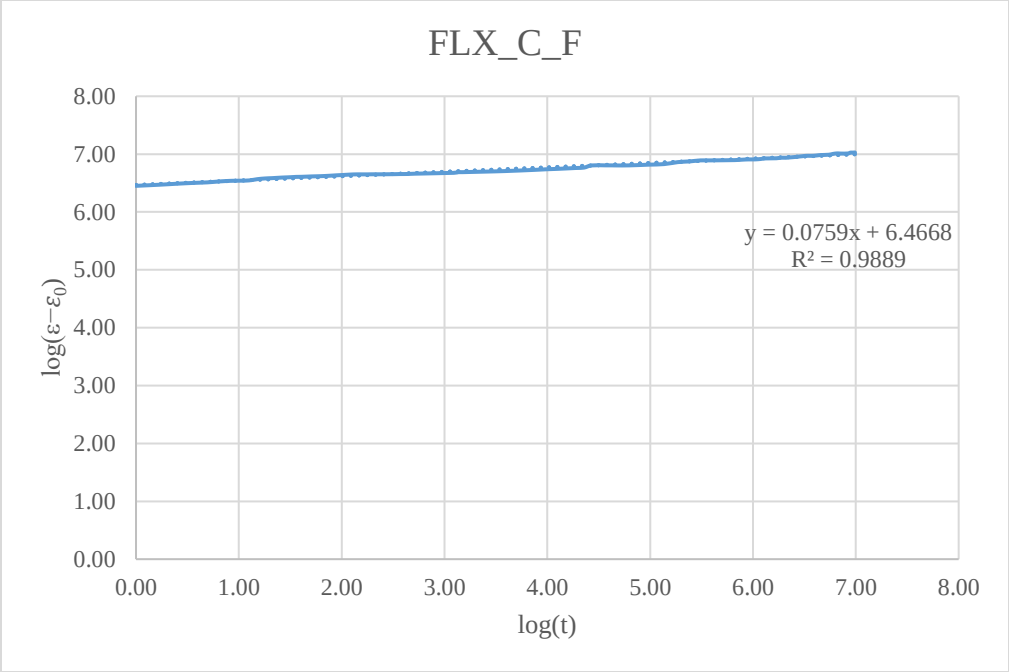

Figure A.6 Plot of log(ε−ε_0) to log(t) of FLX_C_F

BIBLIOGRAPHY

American Society of Civil Engineers. (ASCE). (1984). *Structural Plastics Design Manual*. American Society of Civil Engineers manuals and reports on engineering practice, No.63, ASCE, New York.

ASTM Standard D2990-09 (2009), *Standard Test Methods for Tensile, Compressive, and Flexural Creep and Creep-Rupture of Plastics*, ASTM International, West Conshohocken, PA

ASTM Standard D6272-10 (2010), *Standard Test Method for Flexural Properties of Unreinforced and Reinforced Plastics and Electrical Insulating Materials by Four-Point Bending*, ASTM International, West Conshohocken, PA

ASTM Standard D3917-94 (1994), *Standard Specification for Dimensional Tolerance of Thermosetting Glass-Reinforced Plastic Pultruded Shapes*, American Society for Testing and Materials. ASTM International, West Conshohocken, PA

Bank, L. C., Mosallam, A. S., & Gonsior, H. E. (1990, August). Beam-to-column connections for pultruded FRP structures. *In Serviceability and Durability of Construction Materials*: (pp. 804-813). ASCE.

Mosallam, A. S., & Bank, L. C. (1991). Creep and recovery of a pultruded FRP frame. *In Advanced Composites Materials in Civil Engineering Structures*: (pp. 24-35). ASCE.

Bank, L. C., and A. S. Mosallam. "Creep and failure of a full-size fiber-reinforced plastic pultruded frame." *Composites Engineering* 2.3 (1992): 213217-215227.

Barbero, E., & Tomblin, J. (1992). Buckling testing of composite columns. *AIAA journal*, 30(11), 2798-2800.

Bažant, Z. P., & Cedolin, L. (2010). *Stability of structures: elastic, inelastic, fracture and damage theories*. World Scientific.

Bennett, E. A. (2005). Influence of Creep on the Stability of Pultruded E-Glass. *Polyester Composite Columns at elevated service Temperatures*, Georgia Institute of Technology.

Chambers, A. J., & Antonia, R. A. (1984). Atmospheric estimates of power-law exponents M and M θ. *Boundary-Layer Meteorology*, 28(3), 343-352.

Cottrell, A. H., & Aytekin, V. (1947). Andrade's creep law and the flow of zinc crystals. *Nature*, 160(4062), 328-329.

Cunningham, D., Harries, K. A., & Bell, A. J. (2015). Open-hole tension capacity of pultruded GFRP having staggered hole arrangement. *Engineering Structures*, 95, 8-15.

Daniali, S. (1991, February). Short-term and long-term behavior of two types of reinforced plastic beams. In 46th Annual Conference, *Composites Institute*.

Findley, W.N. and Khosla, G. (1956), "An Equation for Tension Creep of Three unfilled Thermoplastics," *Society of Plastics Engineers* – Journal, Vol. 12, No. 12, pp. 20-25.

Hashem, Z. A., & Yuan, R. L. (2001). Short vs. long column behavior of pultruded glass-fiber reinforced polymer composites. *Construction and Building Materials*, 15(8), 369-378.

Hewson, P. (1978). Buckling of pultruded glass fibre-reinforced channel sections. *Composites*, 9(1), 56-60.

Holmes, M., & Rahman, T. A. (1980). Creep behaviour of glass reinforced plastic box beams. *Composites*, 11(2), 79-85.

Horvath, J. S. (1998). Mathematical modeling of the stress-strain-time behavior of geosynthetics using the Findley equation: General theory and application to EPS-Block geofoam. New York: *Civil Engineering Department*, 35.

Kang, J.O. (2001), Fiber Reinforced Polymeric Pultruded Members Subjected to sustained Loads, Ph.D. Dissertation, Georgia Institute of Technology.

Leaderman, H. (1939). Creep, Elastic Hysteresis and Damping in Bakelite Under Torsion. *Journal of Applied Mechanics*, 6, A79-A85.

Lee, D. J., & Hewson, P. J. (1978). The use of fiber-reinforced plastics in thin-walled structures. Stability Problems in Engineering Structures and Components. New York: *Elsevier Applied Science*, 23-55.

McClure, G., & Mohammadi, Y. (1995). Compression creep of pultruded E-glass-reinforced-plastic angles. *Journal of materials in civil engineering*, 7(4), 269-276.

Mottram, J. T. (1993). Short-and long-term structural properties of pultruded beam assemblies fabricated using adhesive bonding. *Composite Structures*, 25(1-4), 387-395.

Pao, Y. H., & Marin, J. (1952). Deflection and stresses in beams subjected to bending and creep. *JOURNAL OF APPLIED MECHANICS-TRANSACTIONS OF THE ASME*, 19(4), 478-484.

Schapery, R. A. (1969). On the characterization of nonlinear viscoelastic materials. *Polymer Engineering & Science*, 9(4), 295-310.

Scott, D. W., & Zureick, A. H. (1998). Compression creep of a pultruded E-glass/vinylester composite. *Composites Science and Technology*, 58(8), 1361-1369.

Southwell, R. V. (1932, April). On the analysis of experimental observations in problems of elastic stability. In *Proceedings of the Royal Society of London A: Mathematical, Physical and Engineering Sciences* (Vol. 135, No. 828, pp. 601-616). The Royal Society.

Vieira, J., Liu, T. and Harries, K.A. (2017) Flexural Stability of Pultruded GFRP I-Sections, *ICE Structures and Buildings*

Zureick, A., & Scott, D. (1997). Short-term behavior and design of fiber-reinforced polymeric slender members under axial compression. *Journal of Composites for Construction*, 1(4), 140-149.